Measurement of Antenna Performance in Analog LMR Systems Using PL Tone Analysis

Akshay Kumar

Thesis submitted to the Faculty of the
Virginia Polytechnic Institute and State University
in partial fulfillment of the requirements for the degree of

Master of Science
in
Electrical Engineering

S. W. Ellingson, Chair
A. A. (Louis) Beex
T. C. Clancy

December 21, 2012
Blacksburg, Virginia

Keywords: Antennas, Antenna performance, *in-situ* measurements, LMR systems, RF SNR, Public Safety Radio

Measurement of Antenna Performance in Analog LMR Systems Using PL Tone Analysis

Akshay Kumar

ABSTRACT

We are interested in measuring the *in situ* antenna performance in analog land mobile radio (LMR) FM systems. The gain (efficiency and directivity) and self-impedance of an antenna sufficiently characterize its performance and a number of traditional methods exist to measure these quantities. However it is hard to do antenna gain measurements using these methods. Furthermore, it turns out that volumetric antenna gain measurements are not quite relevant for understanding *in situ* performance. In this thesis, we present a novel approach for directly measuring the *in situ* performance of antennas in analog LMR systems. The procedure involves receiving an FM signal simultaneously using the antenna under test (AUT) and a reference antenna. Both received signals are demodulated to audio using separate but identical receivers. Then a convenient method for characterizing the audio signal quality is to analyze the private line (PL) tone. The PL tone signal-to-noise ratio (SNR) is calculated by measuring the power of the tone relative to the sub-audio noise power. The PL tone SNR for both antenna systems is compared as it provides a "bottom line" evaluation of the antenna performance. The audio SNR can also be mapped to RF SNR using a theoretical method. From simulation and experimental studies, we conclude that the RF SNR estimated using this technique is within 0.5 dB of the actual value for RF SNR values between +3 and +36 dB. Finally, we demonstrate this procedure in actual *in situ* LMR antenna measurements.

Acknowledgments

This work was supported in part by Award No. 2009-SQ-B9-K012 awarded by the National Institute of Justice, Office of Justice Programs, U.S. Department of Justice. The opinions, findings, and conclusions or recommendations expressed in this thesis are those of the author and do not necessarily reflect those of the Department of Justice.

I owe my deepest gratitude to my advisor, Dr. Steven Ellingson, for his support and patience with me during the research and writing of this work. This thesis would not have been in shape as it is now without his constructive comments and editing. I would also like to thank my committee members Drs. A. A. (Louis) Beex and T. Charles Clancy for their assistance in finalizing this thesis.

I would like to thank my colleagues Joseph Gaeddert, Amuru Sai Dhiraj, Hunter DeJarnette, Venkata Gautham Chavali, Eyosias Imana and Mike Benonis for discussions on various topics on radio communications. Special thanks to Mr. Randall Nealy for his immense help in familiarizing me with various laboratory equipments, designing the test rig for field evaluations and also for providing useful insights on topics related to antennas and working of LMR FM systems. Thanks a lot, Randall.

I am also thankful to my project members, Hank Tillman and Mahmud Harun for developing the antenna tuner and the reconfigurable antennas as components of the test rig used in the field evaluation. Many thanks to the MPRG lab who helped me during my studies and research at Virginia Tech. I would like to specially mention Ms. Nancy Goad and Ms. Hilda Reynolds for their kind support.

The pictures of the test fixture in Figure 5.2 in Chapter 5 were taken by the author in June 2012.

Contents

List of Figures

List of Tables

Chapter 1

Introduction

Desire for interoperability in applications such as public safety [1, 2] and military communication [3] has led to an increasing interest in mobile and portable radios having a multiband tuning range with a single small antenna. Having done the design and construction of a prototype multiband antenna system, it is equally important to characterize the RF performance of the antenna system. We are particularly interested in *in situ* antenna measurements for analog land mobile radio (LMR) FM systems [4]. It is hard to do volumetric antenna pattern (directivity) measurements using traditional methods [5] due to a number of logistical problems. Furthermore, it turns out that the antenna pattern measurements are not quite relevant for *in situ* performance. We need to find an alternative method that provides a "bottom line" evaluation of *in situ* antenna performance.

In this thesis, we present a novel approach for measuring the *in situ* antenna performance of antennas in TIA-603 analog LMR FM systems. The TIA-603 standard sets transmitter and receiver specifications in the LMR radios that employ FM or PM modulation [6]. Figure 1.1 shows the block diagram for our approach. LMR systems typically have a private line (PL) tone along with the voice message to suppress the interference which would otherwise break squelch in the receiver. In our method, we use this PL tone to estimate and compare the audio and RF SNR of the test antenna system against a reference antenna.

The remainder of this chapter is organized as follows. Section 1.1 summarizes traditional antenna measurement techniques and their limitations. To overcome these limitations, we propose the alternative approach for antenna measurements in Section 1.2. Section 1.3 summarizes the research contributions of this thesis, and Section 1.4 describes the organization

of the remainder of this thesis.

1.1 Traditional Antenna Measurement Techniques

This section summarizes traditional methods used to measure antenna performance and the limitations associated with them. The gain (efficiency and directivity) and self-impedance of an antenna sufficiently characterize its performance. It is quite easy to measure the *in situ* self-impedance of an antenna using a portable vector network analyzer or a hand-held spectrum analyzer (along with a VSWR bridge and power divider) but it is not easy to measure gain (directivity and efficiency).

A common method used for gain (efficiency and directivity) measurement is the gain comparison method in which pre-calibrated standard gain antennas are used to determine the absolute gain of the antenna under test (AUT) [5, 7, 8]. This method requires that the standard antenna should have a high degree of dimensional stability and also, for accurate results, its gain should not be too different from that of the AUT. Another method for gain measurement is the generalized three antenna method [7, 8]. This method, unlike the gain comparison method, does not require *a priori* knowledge of the transmitting or receiving antenna gain. However, both these methods require a lot of tedious mechanical operations such as rotating the AUT with respect to the source antenna using positioners for a volumetric characterization of antenna gain. Furthermore, the far-field criterion for measurements results in large separation between transmitter and receiver which necessitates use of high towers to reduce the power of specular reflection at the receiver. Besides these issues, there are also a number of other logistical problems such as problems with the portability of RF gear, high costs for using antenna ranges and availability of the required RF instrumentation.

We conclude that it is quite hard to do volumetric antenna gain measurements using the traditional methods. Furthermore, we also note that the volumetric gain measurements are not quite relevant for measurement of *in situ* antenna performance in LMR systems. This is because the LMR antennas may be mounted on vehicles and so the antenna gain measurements made for a stationary receiver would be different from the actual gain values when the vehicle is moving. Thus we would like to find an alternative method that provides a "bottom line" evaluation of *in situ* antenna performance for the case of stationary or slowly-varying channel conditions.

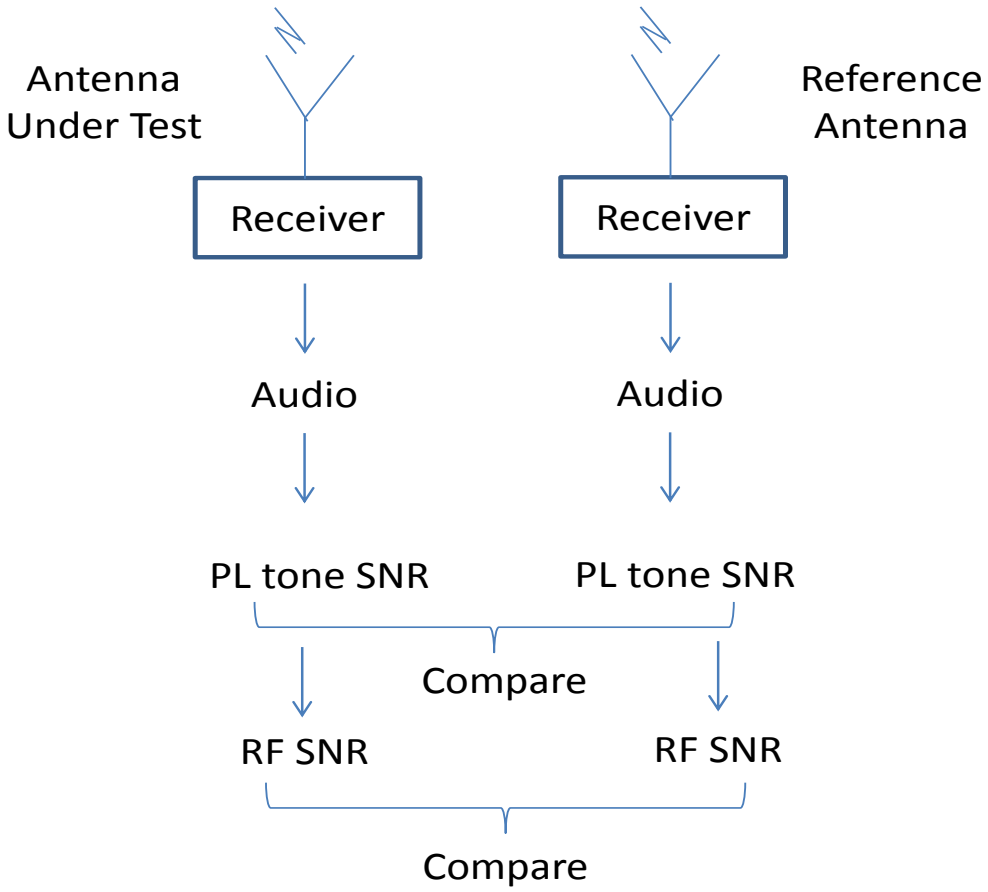

Figure 1.1: Block diagram of our proposed method for *in situ* antenna measurements.

1.2 Proposed *in situ* Measurement Method

In this section, we describe a novel approach for measuring the *in situ* antenna performance in TIA-603 analog LMR FM systems. A block diagram of our approach was shown earlier in Figure 1.1. The procedure starts with receiving an FM signal simultaneously using the AUT and a reference antenna. The reference antenna will typically be a commercial LMR antenna whose performance is already known and is considered satisfactory. Both received signals are then demodulated to audio using separate but identical receivers. The next step is to acquire the audio signal and determine the audio SNR. LMR systems usually have a PL tone injected in the sub-audio band (below 300 Hz) along with the voice message before transmission. We can use the existing PL tone to get an audio SNR metric independent of the voice signal (this is not possible using the voice signal itself, since unlike the PL tone the waveform is not known in advance). For this, the audio output is passed through a digital filter that removes the voice signal, leaving behind the PL tone and the associated sub-audio noise. The PL tone SNR is then calculated by measuring the power of the tone and the sub-audio noise power separately. Specifically, the PL tone SNR is measured using either the parametric estimation and subtraction (PE/S) method or the method of kurtosis as described in Sections 3.1 and 3.2 respectively. The PL tone SNRs provide a "bottom line" evaluation of the antenna performance and can be compared to the same result obtained from a reference antenna for an indication of relative quality. The PL tone SNR may also be mapped to RF SNR using a theoretical result proposed by Jakes (1993) [9, Chapter 4].

1.3 Contributions

The specific contributions of this work include the following items:

- A novel method for *in situ* evaluation of LMR analog FM systems using PL tone analysis as described in Figure 1.1.
- A method for characterization of the audio quality from the recorded audio signals is presented in Chapter 3 ("Characterization of Audio SNR from PL Tone Analysis"). Comparison of the audio SNR metric for the AUT and reference antenna provides a "bottom line" assessment of the antenna performance relative to a known antenna.
- The theoretical result proposed by Jakes in [9, Chapter 4] is used to estimate the pre-

detection (RF) SNR from the audio SNR. The accuracy of the estimated predetection SNR is studied by comparing it with the simulation and experimental predetection SNR. We conducted a series of experiments consisting of laboratory evaluations as well as demonstrations using actual off-the-air LMR signals. The results are presented in Chapter 4 ("Estimation of Predetection SNR from Audio SNR").

- Finally in Chapter 5 ("Field Evaluation of the LMR Multiband Antenna System"), an experimental setup is designed and evaluated to demonstrate the methodology.

1.4 Organization of this Thesis

The remainder of this thesis is organized as follows: Chapter 2 ("System Model and Relevant Theory") presents the system model of the FM communication system and the propagation channel used in our work. Chapter 3 ("Characterization of Audio SNR from PL Tone Analysis") details the method used to characterize audio quality from recorded FM signals. A comparative analysis of these methods using simulations and experimental data is also presented in the same chapter. Having characterized the audio SNR, it is then used to estimate the predetection SNR as described in Chapter 4 ("Estimation of Predetection SNR from Audio SNR"). Then the accuracy of the estimated predetection SNR is studied by comparing it with the simulation and experimental predetection SNR. Chapter 5 ("Field Evaluation of the LMR Multiband Antenna System") demonstrates our proposed method by using it to evaluate an experimental antenna system. Finally in Chapter 6 ("Conclusions"), we summarize the findings of this thesis and suggest future work.

Chapter 2

System Model and Relevant Theory

A method for *in situ* characterization of antenna performance in LMR analog FM systems was proposed in Chapter 1. In order to evaluate the accuracy of our proposed method through simulations, we need to model the FM communication system and the propagation channel in LMR analog FM systems. Section 2.1 ("LMR Systems and the TIA-603 Standard") provides an overview of LMR systems and the TIA-603 standard. The TIA-603 standard determines the transmitter and receiver specifications in LMR radios [6]. A simulation model for a LMR system is presented in Section 2.2 ("System Model"). A theoretical result to determine the audio SNR from the predetection SNR assuming an AWGN channel is presented in Section 2.3 ("Relationship Between Audio SNR and Predetection SNR (AWGN channel)"). A similar result assuming a Rayleigh fading channel is presented in Section 2.4 ("Relationship Between Audio SNR and Predetection SNR (Fading channel)").

2.1 LMR Systems and the TIA-603 Standard

An LMR system is a wireless communication system intended for use by terrestrial users in vehicles (mobiles) or on foot (portables) [10]. LMR systems are used by emergency first responder organizations, public works organizations, and companies with vehicle fleets or field staff. In this thesis, we restrict our discussion to LMR systems employing FM modulation for transmission of voice. Table 2.1 shows the frequency bands of interest for LMR analog FM systems. The TIA-603 standard specifies the characteristics such as modulation scheme, transmission bandwidth etc. that radios must conform to [6]. The TIA-603 standard has

been revised several times namely as revisions A, B, C and D. Table 2.2 shows the TIA-603-B spacing, frequency deviation, and the maximum bandwidth permissible for the frequency bands listed in Table 2.1.

A private line (PL) tone system was introduced in the LMR radios primarily to suppress the interference which would otherwise break squelch in the receiver. In this system, a sub-audio (below 300 Hz) tone, called the PL tone, is generated and added into the transmitter audio. The PL tone is chosen from a set of 50 tones ranging from 67 Hz to about 250 Hz. The receiver has a tone detector circuit and the receiver squelch doesn't open unless the tone is present.

This tone is demonstrated in Figures 2.1 and 2.2. We recorded an audio signal by tuning a ICOM IC-PCR1500 radio receiver to a local UHF-band police transmission. The center frequency of the transmission was 453.2 MHz. Figure 2.1 shows the dynamic spectrum of the recorded audio. The PL tone (at 162.2 Hz) is clearly visible in the spectrum throughout the duration of the signal except for small durations of approximately 0.1 s when one speaker switches to the other. We also observe that the voice spectrum extends from roughly 300 Hz to 3500 Hz. The average PSD of the filtered audio output is shown in Figure 2.2 which again indicates the presence of PL tone along with the voice spectrum.

2.2 System Model

In this section, we develop a mathematical representation of the LMR analog FM system described in Section 2.1 as a tool for later sections of this thesis to evaluate our proposed method through simulations. Figure 2.3 shows our system model. Sections 2.2.1, 2.2.2, and 2.2.3 present the mathematical models for the FM transmitter, propagation channel, and the FM receiver respectively.

2.2.1 Modeling the Transmitter

There are two inputs to the transmitter – the message signal and the carrier. The message signal, $m(t)$, consists of the audio signal and the PL tone. The FM modulator varies the carrier frequency, f_c, in proportion to the amplitude of the message signal. If $c(t) = A_c\ cos(2\pi f_c t)$

Table 2.1: Frequency bands of interest for LMR analog FM systems.

Band	Frequency Range	
	Lo [MHz]	Hi [MHz]
VHF Lo	25.0	50.0
VHF Hi	138.0	174.0
220 MHz	220.0	222.0
UHF	406.1	512.0
700 MHz	764.0	776.0
800 MHz	806.0	817.0

Table 2.2: Modulation parameters for different frequency bands in the TIA-603-B standard.

Band	Simplex -or- Reverse (MS Tx)		TIA-603-B Spacing [kHz]	TIA-603-B deviation +/- [kHz]	TIA-603-B Max. BW [kHz]
	Lo [MHz]	Hi [MHz]			
VHF Lo	25.0	50.0	20	5.0	20.0
VHF Hi	138.0	174.0	25 & 30	5.0	20.0
			12.5 & 15	2.5	11.0
220 MHz	220.0	222.0	5	N/A (Not TIA-603-B)	N/A
UHF	406.1	512.0	25	5.0	20.0
			12.5	2.5	11
700 MHz	764.0	776.0	25 & 12.5	5 & 2.5	25 & 12.5
800 MHz	806.0	817.0	25	5	20

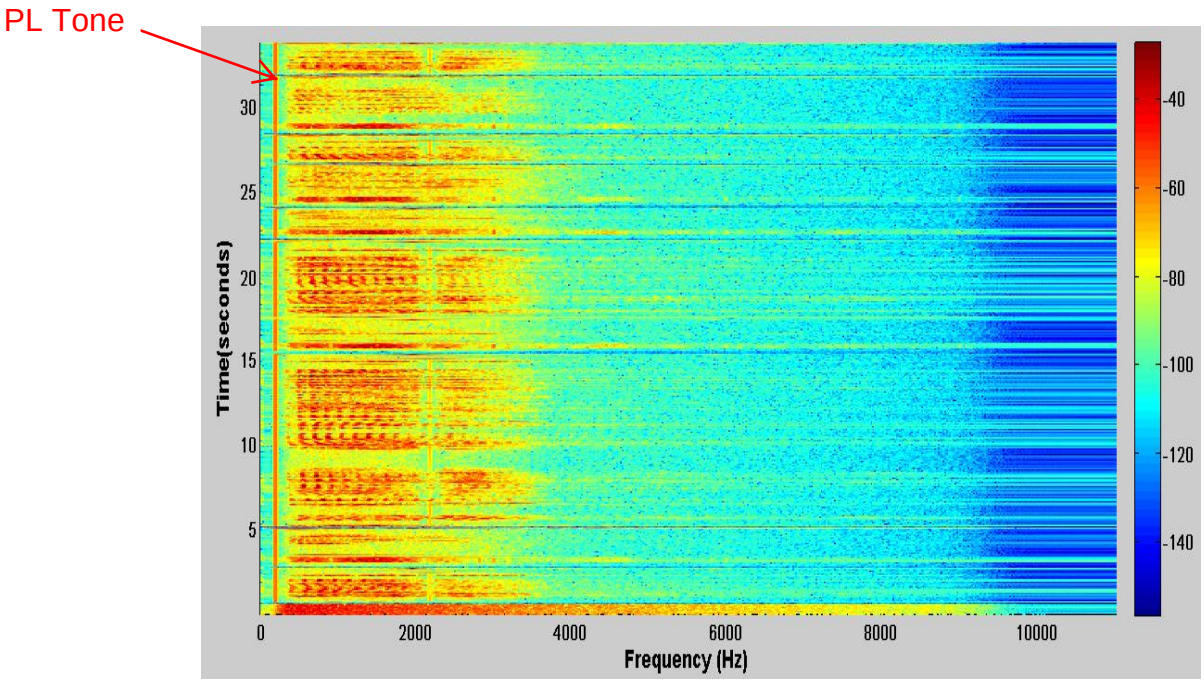

Figure 2.1: Dynamic spectrum of the audio signal described in the text. In this case, the PL tone frequency is 162.2 Hz.

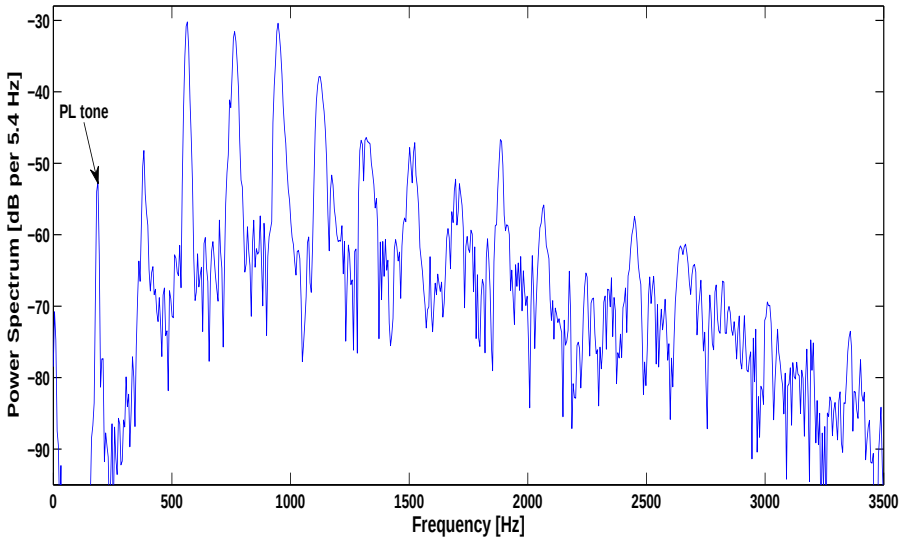

Figure 2.2: Power spectrum of the recorded audio signal described in the text with integration time of 10 ms.

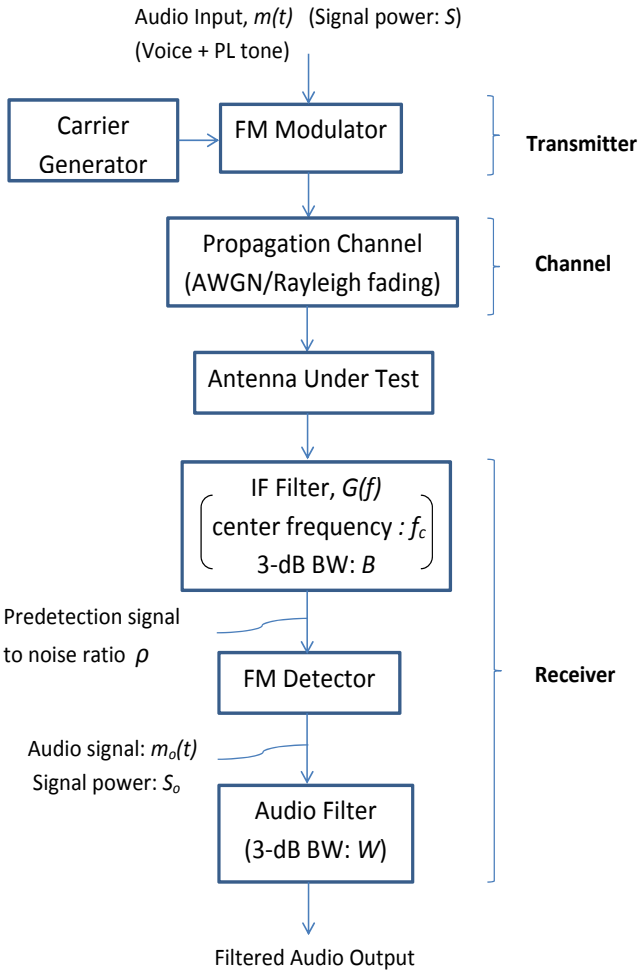

Figure 2.3: System Model

is the carrier, then the modulated signal is given by

$$s_{FM}(t) = A_c \; cos(2\pi f_c t + k_{fm} \int_{-\infty}^{t} m(t)dt), \tag{2.1}$$

where

$$k_{fm} = \frac{2\pi\Delta f}{m_p} \tag{2.2}$$

is the modulation index. Δf is the maximum frequency deviation, and m_p is the maximum amplitude of $m(t)$. The complex baseband representation of the FM modulator in Equation (2.1) is

$$s_{FM,bb}(t) = A_c e^{(jk_{fm}\int_{-\infty}^{t} m(t)dt)}. \tag{2.3}$$

Figure 2.4 shows power spectral density (PSD) of a typical tone-modulated FM signal generated according to the above model.

2.2.2 Modeling the Propagation Channel

We now consider the properties of the propagation channel between the transmit and receive LMR systems. Since LMR systems are intended for use by users either in vehicles or on foot, the relative velocity between the transmitter and receiver can possibly be non-zero in which case the received signal would include time-varying multipath components resulting in a fading scenario. Even if the relative velocity between transmitter and receiver is zero, the propagation environment may not be stationary, again resulting in a fading channel. Hence, our model assumes that the transmitted signal is distorted by a Rayleigh fading channel, and then additive white Gaussian noise (AWGN) is added to it.

Jakes in [9, Chapter 1] proposed a model for generating Rayleigh fading based on the sum-of-sinusoids method. Dent et al. (1993) later improved the original Jakes model in [11]. We use this model to simulate the Rayleigh fading channel. The model assumes that N equal-strength rays arrive at the receiver with uniformly distributed arrival angles α_n, such that the ray n experiences a Doppler shift $\omega_n = \omega_m cos(\alpha_n)$, where $\omega_m = 2\pi f_c v/c$ is the maximum Doppler shift, v is the relative speed of receiver with respect to the transmitter,

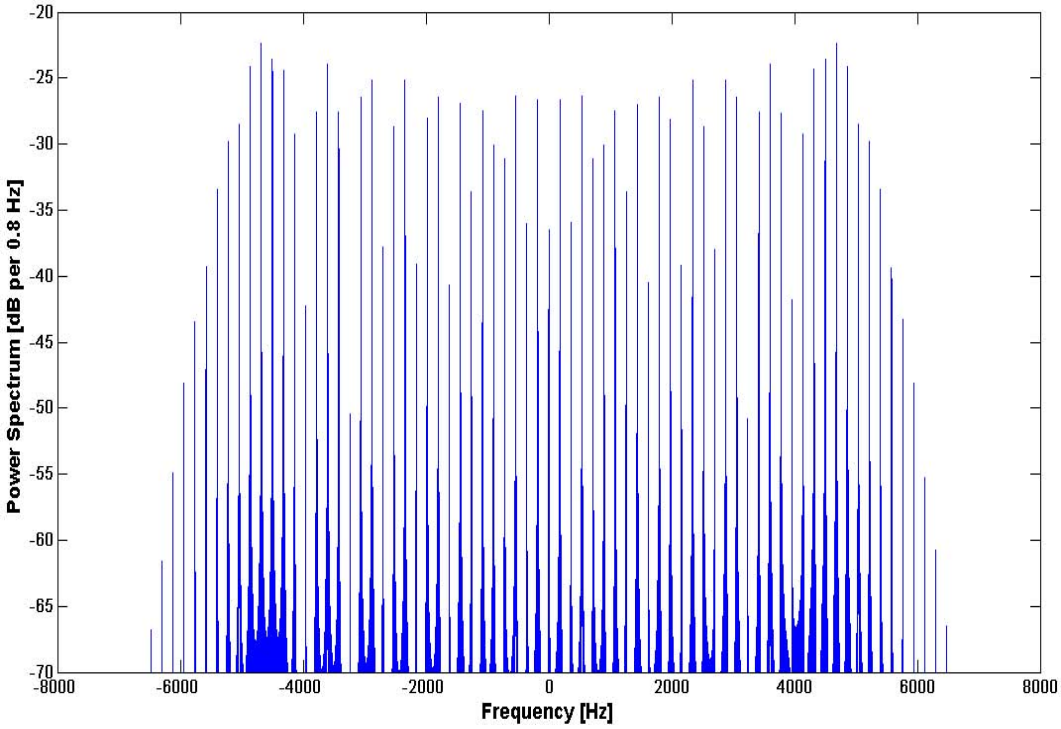

Figure 2.4: Baseband power spectral density of a typical tone-modulated FM signal. Δf is set to 5 kHz, in accordance with the TIA-603-B specification for 138–144 MHz VHF-Hi band listed in Table 2.1. A_c and m_p are set to 5 V and 1.5 V respectively.

and c is the speed of light. The resulting channel coefficient is:

$$T(t) = \sqrt{2/N_o} \sum_{n=1}^{N_o} e^{j\beta_n} cos(\omega_n t + \theta_n), \tag{2.4}$$

where $N_o = N/4$ is the number of equal strength complex oscillators needed to produce the multiple waveforms and the normalization factor $\sqrt{2/N_o}$ gives $E[T(t)T^*(t)] = 1$. By using $\beta = \pi n/N_o$, the real and imaginary parts of $T(t)$ have equal power and are uncorrelated. Setting $\alpha_n = 2\pi(n-5)/N$ provides quadrantal symmetry for all of the arriving waveforms. Randomizing θ_n provides different waveform realizations.

The coherence time of a channel, T_c, is an important fading parameter and is defined as the time duration over which the channel impulse response is considered to be approximately stationary. As a rule of thumb, T_c, is calculated as [12]:

$$T_c = \frac{0.846\pi}{\omega_m} \ . \tag{2.5}$$

The computation of T_c using Equation 2.5 requires knowledge of the Doppler shift. If Doppler shift is not known, T_c can be approximated by the average time interval between two consecutive nulls in the fading envelope, τ_{null}, given by [12]:

$$\tau_{null} = \frac{c}{2f_c v} \ . \tag{2.6}$$

We coin a term called normalized Doppler spread, ω_{norm}, defined as

$$\omega_{norm} = \omega_m/\omega_{max}, \tag{2.7}$$

where ω_{max} is the maximum Doppler spread. This allows us to represent all possible fading scenarios by varying a single dimensionless variable (ω_{norm}). In LMR systems ω_{max} is approximately 522 rad/sec, corresponding to $f_c = 860$ MHz and $v = 29$ m/s. Figure 2.5 shows a Rayleigh fading envelope for $\omega_{norm} = 1$; i.e., the fastest expected fading. We note that $\tau_{null} = 6$ ms and hence $T_c \leq 6$ ms.

2.2.3 Modeling the Receiver

At the receiver, a RF signal consists of the transmitted FM signal plus unwanted signals and noise are captured using the antenna. The desired FM signal is extracted from the received signal using an intermediate frequency (IF) filter. The IF filter is a flat-topped band-pass filter, centered at the carrier frequency and with a 3-dB bandwidth, B, equal to the bandwidth of the FM signal approximated by Carson's formula. The filtered IF signal, $r(t)$, is then fed into the FM detector. In general, the output of a FM detector, $m_o(t)$, is given by

$$m_o(t) = \left| \frac{c_o r^{'}(t)}{|r(t)|} \right| \tag{2.8}$$

where c_o is a dimensionless constant and the prime denotes differentiation with respect to time. However, the FM detector can also be implemented as a sequence of DSP operations. Let $r(n)$ represent the discrete-time equivalent of $r(t)$, where n represents discrete time instants. Then if $r_r(n)$ and $r_i(n)$ are respectively the real and imaginary parts of $r(n)$, and we have

$$\begin{aligned}
r_s(n) &= r_i(n)\ r_r(n-1) - r_r(n)\ r_i(n-1), && (2.9)\\
r_c(n) &= r_r(n)\ r_r(n-1) - r_i(n)\ r_i(n-1), && (2.10)\\
g_1(n) &= r_s(n)/r_c(n), && (2.11)\\
g_2(n) &= arc\ tan(g_1(n)), && (2.12)\\
m_o(n) &= g_2(n)/(T\ k_{fm}) && (2.13)
\end{aligned}$$

where $T = 1/f_s$, f_s being the sampling frequency. The output of the FM detector $m_o(n)$ is then passed through an audio filter which in our simulation is a Chebyshev finite impulse response (FIR) low-pass filter of order 803 and with 3-dB bandwidth, W, set to 3.5 kHz. The dynamic spectrum of the audio filter output was shown earlier in Figure 2.1. It indicates the presence of a PL tone (at 162.2 Hz) and the voice spectrum which extends from roughly 300 Hz to 3500 Hz.

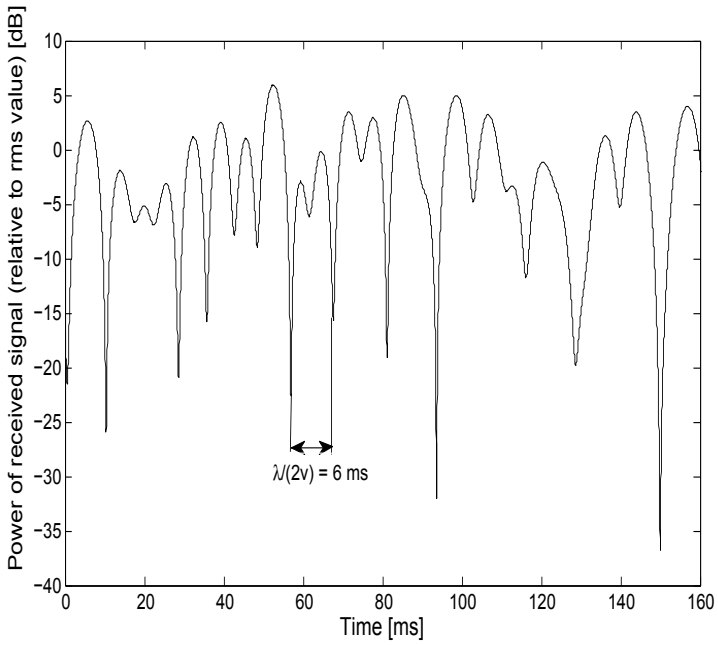

Figure 2.5: Example of a Rayleigh fading envelope for $\omega_{norm} = 1$.

2.3 Relationship Between Audio SNR and Predetection SNR (AWGN channel)

In this section, we present a theoretical expression for the estimation of the audio SNR from the RF SNR under stationary (AWGN) channel conditions. This result is a slightly modified version of the original result proposed by Jakes (1993) [9, Chapter 4]. We make the following assumptions in our model (Figure 2.3):

1. The modulation index for the FM system is greater than unity. This holds true for the TIA-603 modulations.
2. The IF filter has a Gaussian-shaped frequency response, $G(f)$, given by:

$$G(f) = e^{-4\pi(f-f_c)^2/9B^2} \ . \tag{2.14}$$

   We lose little generality by making this assumption since the audio filter bandwidth is usually narrow relative to the IF bandwidth.

As the IF SNR falls and goes below the threshold, the signal modulation is suppressed. So the signal output from the detector, $m_o(t)$, is given by [9, Chapter 4], [13]:

$$m_o(t) = m(t)(1 - e^{-\rho}), \tag{2.15}$$

where ρ is the predetection SNR (at the output of the IF filter). Hence the output baseband signal power, S_o, is related to the input modulation signal power, S_i, as:

$$S_o = (1 - e^{-\rho})^2 S_i. \tag{2.16}$$

Let k denote the transfer characteristic (gain) of the detector. $k = 2\pi k^{'}$, where $k^{'}$ is a constant with units of Hz/V. Let σ_m denote the RMS frequency deviation of the signal $k^{'}m(t)$. Hence its power is σ_m^2. Then the IF bandwidth used is chosen according to the formula $B = 2(W + \sigma_m\sqrt{10})$, where W is the cutoff frequency of the low pass audio filter. This ensures that modulation peaks less than $\sigma_m + 10$ dB are contained within the deviation given by Carson's rule for sinusoidal modulation. Thus we have,

$$\begin{aligned} S_i &= \frac{\sigma_m^2}{k^{'2}}, & (2.17)\\ &= \frac{4\pi^2\sigma_m^2}{k^2}, & (2.18)\\ &= \frac{\pi^2(B - 2W)^2}{10k^2}. & (2.19) \end{aligned}$$

Rice in [14] divided the one-sided baseband noise spectrum, $P(f)$, into three components:

$$P(f) = P_1(f) + P_2(f) + P_3(f). \tag{2.20}$$

$P_1(f)$ has the same spectrum shape as the output noise spectrum when the carrier is absent. $P_2(f)$ has the shape of the output noise spectrum when the carrier is very large,

$$P_2(f) = (1 - e^{-\rho})^2 P_{m_o}(f), \tag{2.21}$$

where $P_{m_o}(f)$ is the output noise spectrum when $\rho \gg 1$, and is given by [9, Chapter 4]:

$$P_{m_o}(f) = \frac{2\pi^2 f^2 e^{-4\pi(f-f_c)^2/9B^2}}{k^2 B\rho}. \tag{2.22}$$

$P_3(f)$ is a correction term that predominates in the threshold region of ρ. Davis in [13] has shown that in the frequency range from 0 to W, where $W < B$, the spectral components $P_1(f) + P_3(f)$ may be accurately approximated by

$$P_D(f) \approx 8\pi B e^{-\rho} \left[k^4 \sqrt{2(\rho + 2.35)}\right]^{-1/2}. \tag{2.23}$$

The above approximations may be combined to provide an approximation for the overall baseband noise spectrum:

$$\begin{aligned} P(f) &\approx (1 - e^{-\rho})^2 P_{m_o}(f) + P_D(f) && (2.24)\\ &\approx \frac{\left[2\pi f(1 - e^{-\rho})\right]^2 e^{-4\pi(f-f_c)^2/9B^2}}{k^2 B\rho} + \frac{8\pi B e^{-\rho}}{k^2\sqrt{2(\rho + 2.35)}} && (2.25) \end{aligned}$$

The total noise power, N, out of a rectangular baseband audio filter is given by:

$$\begin{aligned} N(\rho) &= \int_0^W P_2(f)df + \int_0^W P_D(f)df, && (2.26)\\ &= \frac{a(1 - e^{-\rho})^2}{k^2\rho} + \frac{8\pi BW e^{-\rho}}{k^2\sqrt{2(\rho + 2.35)}}, && (2.27) \end{aligned}$$

where using the Maclaurin series expansion, a is given by

$$\begin{aligned} a &= \frac{4\pi^2}{B}\int_0^W f^2 e^{-4\pi(f-f_c)^2/9B^2}df, && (2.28)\\ &= \frac{4\pi^2 W^3}{3B}\left\{1 - \frac{4\pi}{15}\left(\frac{W}{B}\right)^2 + \frac{8\pi^2}{189}\left(\frac{W}{B}\right)^4 + \cdots\right\}. && (2.29) \end{aligned}$$

Since we have assumed that the modulation index is greater than unity, W is much smaller than B. Therefore, we will consider only first three terms in the Equation (2.29) and still get a fairly accurate value of a. Assuming unit impedance, we find that Equations (2.19) and (2.27) have the correct units. Now the audio SNR is simply the ratio S_0/N.

Thus the procedure for obtaining the audio SNR from predetection SNR, ρ, is as follows:

1. Modulation signal power, $S_i = \left(\pi^2 (B - 2W)^2\right)/(10k^2)$. Since k cancels out in the expression for the audio SNR, we can choose any value for k. We choose $k = 1$ here.

2. Audio signal power, $S_0 = (1 - e^{-\rho})^2 S_i$.
3. Compute the audio noise power, N using Equations (2.27) and (2.29). For calculating a, consider only first three terms in Equation (2.29).
4. Audio SNR, $\text{SNR}_{a,AWGN} = S_0/N$.

Figure 2.6 shows a plot of the audio SNR as a function of predetection SNR determined using this method.

2.4 Relationship Between Audio SNR and Predetection SNR (Fading Channel)

In the last section, a theoretical relationship between audio SNR and predetection SNR was presented assuming a stationary AWGN channel. However as explained earlier in Section 2.2.2, the propagation channel in LMR systems is often time-varying resulting in multipath fading at the receiver. Therefore in this section, we present the relationship between the audio SNR and the predetection SNR for a Rayleigh fading channel. We investigate the following scenarios:

2.4.1 Slowly-Varying Channel

For a slowly-varying channel, the coherence time is long enough to easily select a reasonable integration time (of order of magnitude of 100 ms) for tone estimation that is less than the coherence time. In that case, the channel can be treated as approximately stationary over the selected integration time. Then using the techniques described in Sections 3.1 and 3.2, the audio SNR is estimated independently for a number of signal segments each of duration equal to the integration time and is then averaged to get the average audio SNR. Finally using the theoretical result in Section 2.3, we determine the average predetection SNR from the average audio SNR.

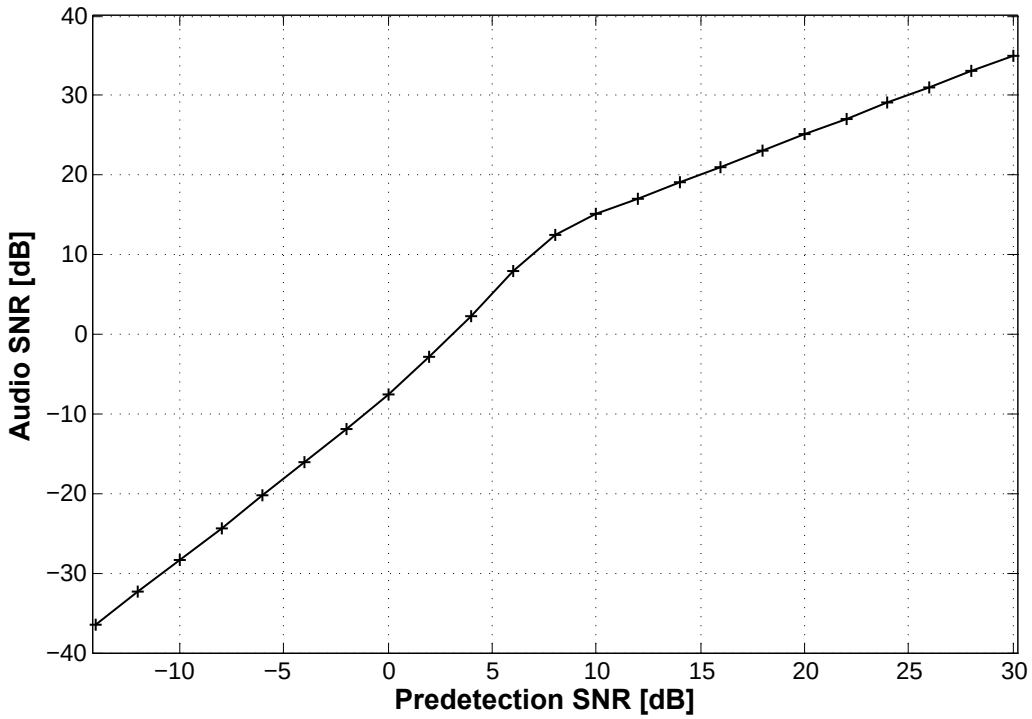

Figure 2.6: Relationship between audio SNR and predetection SNR using the theoretical result (Non-fading channel). B and W are set to 17 kHz and 3.5 kHz respectively.

2.4.2 Rapidly-Varying Channel

In the case of a rapidly-varying channel, it is difficult to choose a reasonable integration time (of order of magnitude of 100 ms) for tone estimation that is less than the coherence time of the channel. However if the integration time is chosen to be small enough to be less than the coherence time, then the approach described in Section 2.4.1 can be used to determine the audio and predetection SNR. If that is not the case, the channel cannot be assumed to be stationary over the selected integration time. As a result, it is not possible to use the audio SNR estimation techniques (Section 3.1 and 3.2) and the theoretical result (Section 2.3) to determine the audio and predetection SNR.

For all of our work in this thesis, the propagation channel is assumed to be either AWGN or slowly-varying. However, for reference purposes, we present here a theoretical relationship between audio SNR and predetection SNR for a rapidly-varying channel as proposed by Jakes in [9, Chapter 4].

The average audio signal power, $\bar{S}_o$, is given by

$$\bar{S}_o = \left(\frac{\rho_o}{1+\rho_o}\right)^2 S_i \ , \tag{2.30}$$

where ρ_o is the average predetection SNR and S_i is the input modulation signal power given by Equation 2.19.

The audio noise consists of four components: (1) the noise due to suppression of the signal (N_{sn}), (2) the noise due to random FM caused by fading (N_{rfm}), (3) the usual Gaussian noise present due to the additive noise present at the input (N_{gn}), and (4) the click noise (N_{cn}). The click noise can be ignored, since this effect is significant only in the vicinity of the FM threshold as opposed to well below or well above the threshold. Also it produces relatively small changes in the noise output.

The average audio noise power caused by signal suppression, $\bar{N}_{sn}$, is

$$N_{sn} = S_i \left(\frac{1}{2\rho_o+1} - \frac{1}{(\rho_o+1)^2}\right). \tag{2.31}$$

The Gaussian noise component, $\bar{N}_{gn}$, can be obtained by averaging Equation 2.26 over ρ:

$$\bar{N}_{gn} = \int_0^\infty p(\rho) N(\rho) d\rho \tag{2.32}$$

$$= \frac{a}{\rho_o k^2} log \frac{(1+\rho_o)^2}{(1+2\rho_o)} + \frac{8BW}{k^2} \sqrt{\frac{\pi}{2\rho_o(\rho_o+1)}} e^{2.35(\rho_o+1)/\rho_o} \text{erfc}\left(\sqrt{2.35(\rho_o+1)/\rho_o}\right) \ . \tag{2.33}$$

$\text{erfc}(x) = 1 - \text{erf}(x)$, and $\text{erf}(x)$ is defined as follows:

$$\text{erf}(x) = \frac{2}{\pi} \int_0^x e^{-y^2} dy. \tag{2.34}$$

Assuming a uniform angle of arrival for all the multipaths at the receiver, the random FM output noise, N_{rfm} is given by [15, 16]

$$N_{rfm} = 2\left(\frac{\pi f_c v}{kc}\right)^2 log \frac{W_2}{W_1} \ , \tag{2.35}$$

where c is the speed of light and the audio bandwidth is from W_1 to W_2. For our work, we have W_1 and W_2 set to 350 Hz and 3500 Hz respectively. Note that the random FM output noise is independent of ρ.

So the average audio SNR, $\text{SNR}_{a,fad}$, is given by

$$\text{SNR}_{a,fad} = \frac{\bar{S}_0}{\bar{N}_{sn} + N_{rfm} + \bar{N}_{gn}} \tag{2.36}$$

Figure 2.7 shows a plot of the average audio SNR as a function of average predetection SNR determined using this method for different values of normalized Doppler spread ω_{norm}. For the sake of comparison of results, the theoretical result in Section 2.3 is also plotted on Figure 2.7. Note that the average audio SNR increases almost linearly with the average predetection SNR till it reaches a limiting value. This is because the noise components $\bar{N}_{sn}$ and $\bar{N}_{gn}$ become negligibly small compared to N_{rfm} at high values of average predetection SNR. The limiting audio SNR increases on decreasing ω_{norm} and for $\omega_{norm} = 0$, we note that there is no limiting value for audio SNR because $N_{rfm} = 0$. Further, for $\omega_{norm} = 0$ and $\rho_o > 10$ dB, the slope of the curve is equal to that of the theoretical result for the AWGN channel.

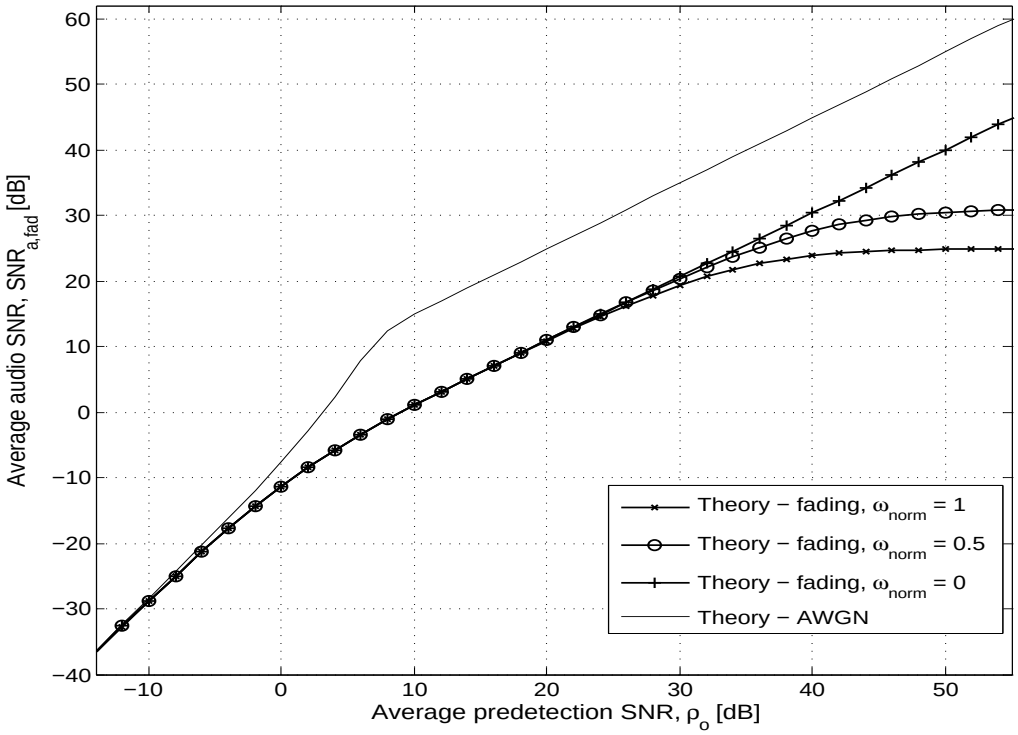

Figure 2.7: Relationship between audio SNR and predetection SNR for different values of ω_{norm} using the result in Section 2.4.2. B and W are set to 17 kHz and 3.5 kHz respectively.

Chapter 3

Characterization of Audio SNR from PL Tone Analysis

The receiver output in the LMR system model presented in Section 2.2 (Figure 2.3) is an audio signal containing the voice message and a PL tone. This is also illustrated in Figure 2.1 which shows the dynamic spectrum of the audio output. Given the audio output, we wish to measure the SNR of the PL tone as it provides a "bottom line" evaluation of the antenna performance. For this, we filter out all but the vicinity of the PL tone. We then measure the SNR of the filtered signal using the parametric estimation and subtraction (PE/S) or the kurtosis method. The PE/S method involves estimation of the parameters (amplitude, frequency and phase) of the tone and then synthesis and subtraction of the tone from the original signal to get noise. The SNR of the filtered signal is then the power of the estimated tone divided by the power of the original signal after PE/S. In the kurtosis method, we estimate the SNR of the filtered signal using a theoretical relationship involving the kurtosis of the filtered signal, the tone and the noise.

The organization of this chapter is as follows. The PE/S and kurtosis methods are described in Sections 3.1 ("Parametric Estimation and Subtraction (PE/S)") and 3.2 ("Method of Kurtosis"). A comparative analysis of the PE/S and kurtosis methods is done first using simulated data in Section 3.3 ("Comparison of PE/S and Kurtosis for Simulated Signals") and then through experiments in Sections 3.4 ("Laboratory Demonstration") and 3.5 ("Demonstration using Actual LMR Signals"). Finally, in Section 3.6 ("Conclusions"), we conclude this chapter with comments on the performance of the PE/S and kurtosis methods.

3.1 Parametric Estimation and Subtraction (PE/S)

This method is suitable for estimating the SNR of a noisy signal when the signal of interest can be described in a simple mathematical form with only a small number of slowly-varying parameters. In our case, we may assume that the PL tone is a sinusoid whose parameters are amplitude, frequency and phase. These parameters are estimated and a noise-free copy is locally synthesized. This estimated signal is then coherently subtracted from the original signal, nominally leaving only noise. The SNR of the noisy signal is then the ratio of power of the estimated signal divided by the power of the original signal after PE/S.

The input signal is modeled as

$$x(t) = s(t) + n(t), \text{ where} \tag{3.1}$$
$$s(t) = ae^{j(\omega t+\theta)}, \tag{3.2}$$

and $s(t)$ is the signal to be estimated having a, ω, and θ as the magnitude, frequency and phase respectively. $n(t)$ is the noise, assumed to be Gaussian. Then the optimal estimates of the parameters a, ω and θ are given by

$$\hat{\omega} = \arg\max_{\omega} \left|\left\langle x(t)e^{-j\omega t}\right\rangle\right|, \tag{3.3}$$
$$\hat{a} = \left|\left\langle x(t)e^{-j\hat{\omega} t}\right\rangle\right|, \tag{3.4}$$
$$\hat{\theta} = \angle\left\langle x(t)e^{-j\hat{\omega} t}\right\rangle, \tag{3.5}$$

where the angle brackets $< . >$ denote time averaging.

As noted in Section 2.2.2, the received radio signal is generally not stationary over long durations of time. This is due to the fading environment; specifically, by time-varying multipath. To accommodate this, we apply the PE/S method repeatedly within short segments of the signal during which it can be assumed to be approximately stationary. An example of this approach is discussed in Lee (2008) [17] in the context of mitigation of RF interference. The duration of the signal segments (or the integration time) used for the PE/S method needs to be decided carefully. It is desired to have integration time as long as possible and preferably much smaller than the coherence time of the channel. This is because increasing the integration time improves our estimate of PL tone SNR but also makes the result less robust to channel variations.

3.2 Method of Kurtosis

In this method, the kurtosis is used to calculate the SNR for the signal, as discussed in Matzner (1994) [18]. In this case, both $s(t)$ and $n(t)$ in Equation (3.1) are assumed to be real, stationary, zero mean and mutually independent; the latter at least with respect to the fourth order statistics.

Since the sum of independent random processes corresponds to the product of the respective characteristic functions, we have:

$$\phi_x(\omega) = \phi_s(\omega)\phi_n(\omega), \tag{3.6}$$

where $\phi_x(\omega)$, $\phi_s(\omega)$, $\phi_n(\omega)$ are the characteristic functions of $x(t)$, $s(t)$, and $n(t)$ respectively. The characteristic function $\phi_x(\omega)$ of a random process $x(t)$ having a probability density function (pdf) $f_X(x)$, is expanded in a series of its moments as:

$$\phi_x(\omega) = \int_{-\infty}^{\infty} f_X(x)e^{-j\omega x}dx = \sum_{k=0}^{\infty}(-j)^k m_{x,k}\frac{\omega^k}{k!}, \tag{3.7}$$

where $m_{x,k}$ is the k-th order moment of $x(t)$. For a discrete signal $x[n]$, $m_{x,k}$ can be computed as:

$$m_{x,k} = \frac{1}{N}\sum_{n=1}^{N}|x[n]|^k \ , \tag{3.8}$$

where N is the sample size.

It requires simple algebra to show using Equations (3.6) and (3.7) that the k-th order moment of the sum $x(t)$ in Equation (3.1) is given by

$$m_{x,k} = \sum_{l=0}^{k}\binom{k}{l}m_{s,l}m_{n,k-l} \ . \tag{3.9}$$

If we evaluate Equation (3.9) for $k = 2$ and $k = 4$ and use the assumption that both signal and noise are zero mean, we find

$$m_{x,2} = m_{s,2} + m_{n,2} \ \text{ and} \tag{3.10}$$

$$m_{x,4} = m_{s,4} + m_{n,4} + 6m_{s,2}m_{n,2} \ . \tag{3.11}$$

The kurtosis K_x of $x(t)$ is defined as

$$K_x = m_{x,4}/m_{x,2}^2 \ . \tag{3.12}$$

Using Equation (3.12) we obtain from Equations (3.10) and (3.11)

$$(K_x - 3) = (K_s - 3)\kappa^2 + (K_n - 3)(1 - \kappa)^2 \ , \tag{3.13}$$

where $\kappa = m_{s,2}/(m_{s,2} + m_{n,2})$ is related to the SNR we seek. To simplify Equation (3.13), let $P = (K_x - 3)$, $Q = (K_s - 3)$, and $R = (K_n - 3)$. Then solving for κ gives us

$$\kappa = (R \pm \sqrt{P(Q + R) - QR})/(Q + R) \tag{3.14}$$

Since the noise is assumed to be Gaussian and the signal, $s(t)$, is a sinusoid (PL tone), $K_n = 3$ and $K_s = 1.5$. So $R = 0$ and $Q = -1.5$. Substituting these values in Equation (3.14), we get

$$\kappa = \sqrt{(3 - K_x)/1.5} \ . \tag{3.15}$$

Now the SNR of the received signal $x(t)$ is given by

$$\text{SNR} = \kappa/(1 - \kappa) \ . \tag{3.16}$$

Summarizing, the procedure for obtaining SNR from the data, $x(t)$, is as follows:

1. Compute the moments $m_{x,4}$ and $m_{x,2}$ using Equation (3.8) for $k = 2$ and $k = 4$ respectively.
2. Determine the kurtosis from Equation (3.12).
3. $\kappa = \sqrt{(3 - K_x)/1.5}$ from Equation (3.15).
4. $\text{SNR} = \kappa/(1 - \kappa)$ from Equation (3.16).

As described in Section 3.1, when the received signal is subjected to a time-varying fading (non-stationary) channel, we partition the received signal into small segments over which it is effectively stationary, and then this method is applied independently to each of these segments. The duration of these signal segments must be chosen carefully as described previously in Section 3.1.

3.3 Comparison of PE/S and Kurtosis for Simulated Signals

In this section, we perform a detailed comparison of the SNR estimation techniques using simulations. We first consider the simplistic case of a sinusoid in white Gaussian noise in Section 3.3.1. Then we add the process of FM modulation and demodulation to this test case in Section 3.3.2. Finally, in Section 3.3.3, we consider a FM system in a Rayleigh fading channel.

3.3.1 Ideal Conditions (No Modulation, AWGN channel)

Since for simulated data the audio SNR can be precisely controlled, this provides us a "baseline" to test the accuracy of the experimental techniques. Consider the case of a sinusoid in white Gaussian noise, corresponding to a time-invariant channel. The frequency of the sinusoid is 180 Hz and its amplitude is varied so that SNR varies from -25 dB to $+10$ dB.

We need to choose the integration time for the PE/S and kurtosis methods prior to estimating SNR. The trade-off in selecting the length of the integration time has been discussed previously in Section 3.1. For a mobile radio channel, coherence time, T_c, varies with the Doppler spread and can be estimated using Equation 2.5. Let us define a "best case" fading scenario over our frequency and velocity range of interest corresponding to a carrier frequency $f_c = 45$ MHz and transmitter velocity $v = 1$ m/s (vehicle almost stationary). This results in $T_c = 2800$ ms. Let us also define a "worst case" fading scenario corresponding to a carrier frequency $f_c = 860$ MHz and transmitter velocity $v = 29$ m/s, which results in $T_c = 5$ ms.

Figures 3.1–3.4 compare the experimental SNR, determined using the PE/S and kurtosis methods, against the actual SNR for integration times of 5 ms, 50 ms, 100 ms, and 2800 ms respectively. It is observed that on increasing the integration time, both methods yield accurate results at lower SNR. For an integration time of 5 ms, PE/S method works well for SNR ≥ -15 dB. On increasing the integration time to 2800 ms, PE/S method gives accurate results for SNR down to about -35 dB. At low SNR values, the kurtosis result flattens out earlier than the PE/S curve. This is because PE/S is statistically optimum for parameter

estimation.

3.3.2 Effect of Modulation/Demodulation (AWGN channel)

Now we add the process of FM modulation and demodulation to this test case as shown in Figure 2.3. The channel is assumed to be AWGN with no fading. In Equation (2.3), the message signal $m(t)$ consists of only PL tone with frequency $f_{pl} = 180$ Hz and amplitude $A_{pl} = 1$. Also $m(t) = 0$ for $t < 0$ s. The amplitude of the carrier, A_c is varied to get a predetection SNR range from -16 dB to 31 dB. Table 2.2 in Chapter 2 lists the modulation parameters for different frequency bands in the TIA-603-B standard. We select the 138–144 MHz VHF-Hi band to use the corresponding modulation parameters in our simulations. Therefore we set the maximum frequency deviation Δf, and the bandwidth of IF filter, B, to 5 kHz and 17 kHz respectively. The selected frequency band does not effect our result in any other way except for the differences in values of modulation parameters because we perform the simulations at baseband.

In Figure 3.5, we plot the audio SNR as a function of predetection SNR using the PE/S method, the kurtosis method, and the theoretical result for audio SNR (Section 2.3). Since the channel is stationary, following from the analysis done in Section 3.3.1, a sufficient integration time for the PE/S method and the kurtosis method is 100 ms. It is observed that the PE/S and kurtosis methods are in close agreement with each other for predetection SNR > 5 dB. The PE/S and kurtosis curves have roughly the same slope as the theoretical curve and follows it with a 1–5 dB offset, for predetection SNR range from 0 dB to 30 dB. The agreement between the PE/S and theoretical result remains pretty good for predetection SNR down to -5 dB with the offset being greater than 5 dB for predetection SNR from -5 to -15 dB.

Whether the agreement between the results is good enough or not is application-dependent. However a possibility is to first determine the audio SNR using the PE/S or kurtosis method and then use Figure 3.5 to calibrate from that to the theoretical result. We however will not be doing this mapping for our work.

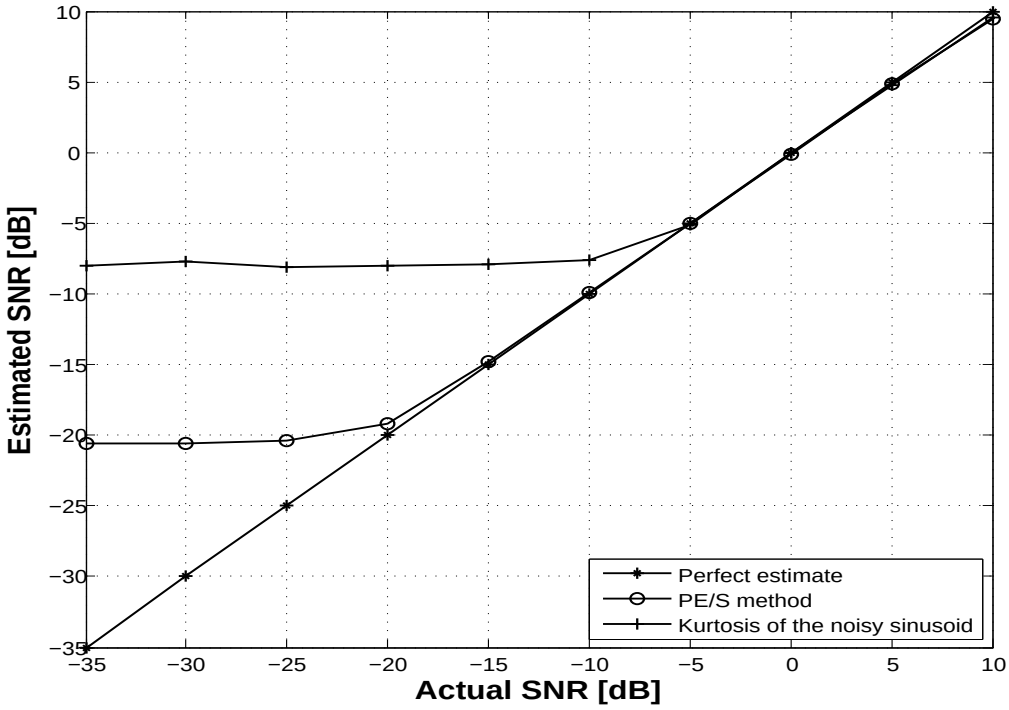

Figure 3.1: Plot of experimental SNR against actual SNR of a noisy sinusoid. Integration time is 5 ms.

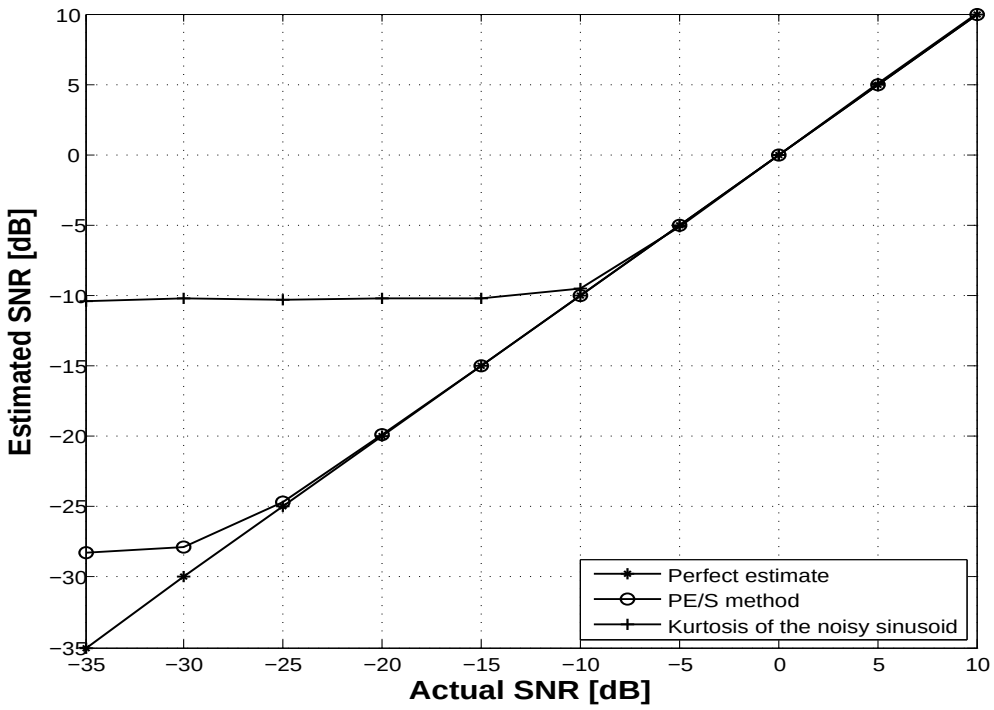

Figure 3.2: Plot of experimental SNR against actual SNR of a noisy sinusoid. Integration time is 50 ms.

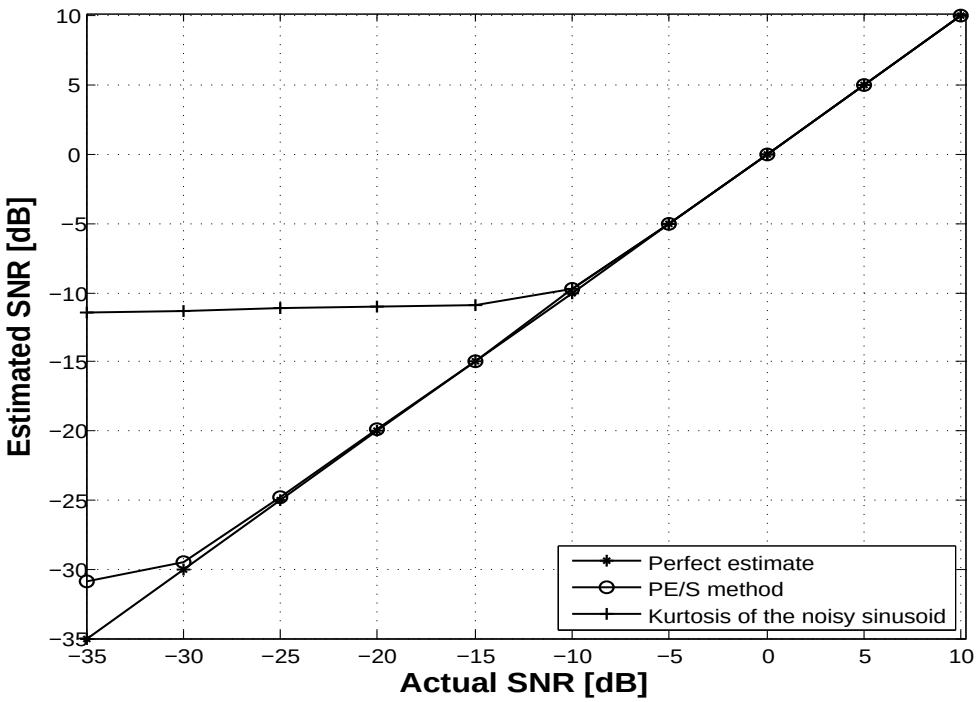

Figure 3.3: Plot of experimental SNR against actual SNR of a noisy sinusoid. Integration time is 100 ms.

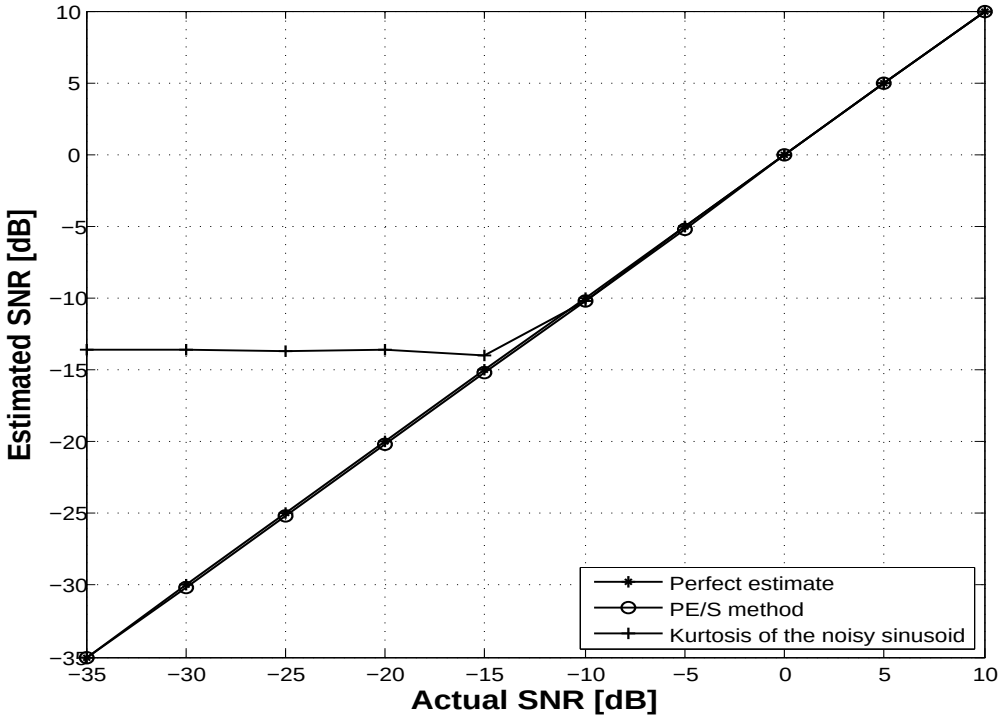

Figure 3.4: Plot of experimental SNR against actual SNR of a noisy sinusoid. Integration time is 2800 ms.

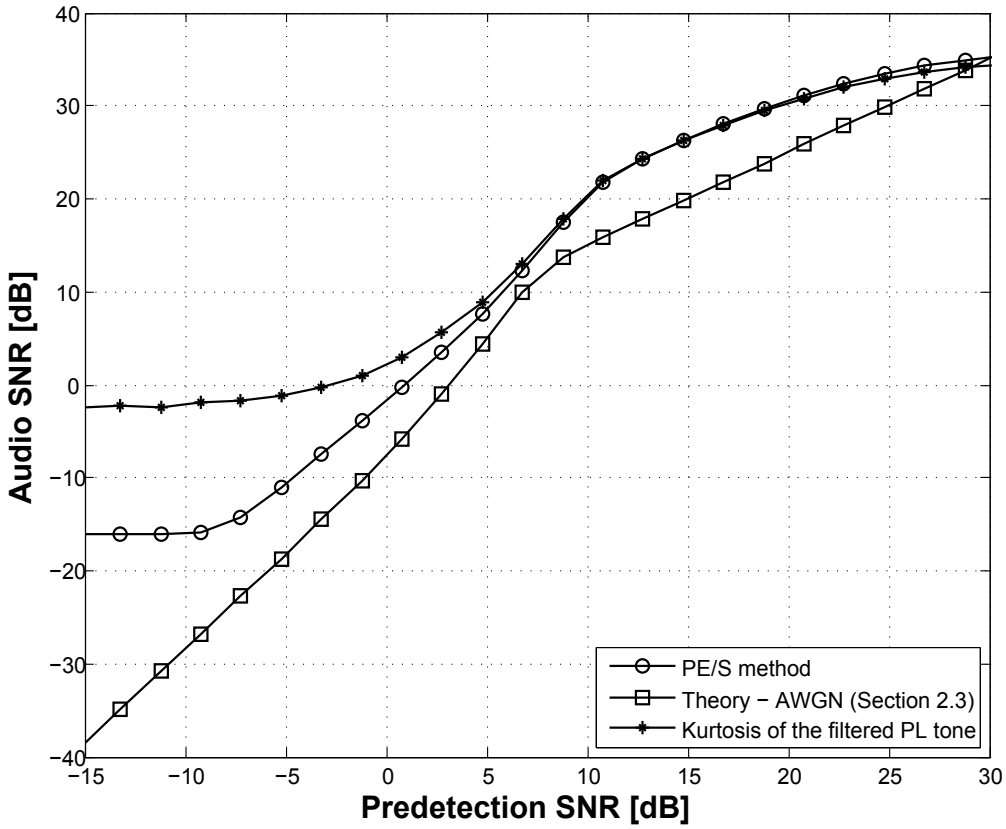

Figure 3.5: Relationship between audio SNR and predetection SNR - PE/S and kurtosis methods (Non-fading channel).

3.3.3 Impact of Rayleigh Fading

Finally we repeat the test case of Section 3.3.2 but now with a time-varying Rayleigh fading channel. Before Equation (2.4) can be used to simulate the Rayleigh fading environment, the parameters of the Jakes model must be determined. N_o is set to 16 and the parameter θ_n is randomly and uniformly distributed between $-\pi$ to π. Let $\tau_{norm} = \tau/\tau_{null}$ represent the normalized integration time, where τ is the selected integration time for the received signal and τ_{null} is the average time interval between two consecutive signal nulls, given by Equation 2.6.

Consider the best- and worst-case fading scenarios as defined in Section 3.3.1 corresponding to $\omega_{norm} \approx 0$ and $\omega_{norm} = 1$ respectively, where ω_{norm} is the normalized Doppler spread given by Equation 2.7. The performance of the PE/S and kurtosis methods for both the cases is summarized in Table 3.1. We measured the root-mean-square (RMS) offset between the simulation and theoretical result (AWGN for $\omega_{norm} = 0$, Rayleigh fading for $\omega_{norm} = 1$) for a predetection SNR range from 5 dB to 25 dB. It is observed that as the integration time is increased from a value much lower than the null-fading period to the null-fading period, the RMS offset between the PE/S result and the theoretical result increases by a few dB. However on making the integration time much larger than the null-fading period, the offset actually decreases significantly since the fading is averaged out. Based on the same logic, the kurtosis result also gets fairly close to theoretical result at higher integration times.

Figures 3.6–3.8 show the audio SNR as a function of predetection SNR using the PE/S method, the kurtosis method, and the theoretical result (AWGN) for $\omega_{norm} \approx 0$ and $\tau_{norm} =$ 0.09, 1, and 5 respectively. Figures 3.9–3.11 show the audio SNR as a function of predetection SNR using the PE/S method, the kurtosis method, and the theoretical result (AWGN and Rayleigh fading) for $\omega_{norm} = 1$ and $\tau_{norm} = 0.93$, 9.3, and 93 respectively.

We conclude this section by analyzing three separate cases for different values of integration time τ as listed below:

1. When $\tau \ll T_c$ ($\tau_{norm} \ll 1$), the channel can be assumed to be stationary over the selected integration time. In this case, the PE/S and kurtosis methods perform fairly well and from Figure 3.6, we note that the RMS offset between the simulation and the theoretical result is low with the slope of all the curves roughly the same.
2. When $\tau \approx T_c$ ($\tau_{norm} \approx 1$), the channel does not have stationary characteristics over

Table 3.1: Effect of different fading characteristics and integration time on the performance of PE/S and kurtosis methods.

Doppler shift, normalized to worst-case Doppler shift (f_c=860 MHz, v=27 m/s)	Integration time τ, normalized to the null-fading period ($c/2f_cv$)	RMS offset from the theoretical result (AWGN for $\omega_{norm} = 0$, Rayleigh fading for $\omega_{norm} = 1$) for the predetection SNR range: 5–25 dB	
		PE/S method	Kurtosis method
0	0.09	5.4 dB	6.3 dB
	1	14.1 dB	4.9 dB
	5	2.8 dB	2.3 dB
1	0.93	11.6 dB	16.2 dB
	9.3	9.0 dB	13.0 dB
	93	6.0 dB	10.5 dB

the selected integration time. This degrades the performance of the PE/S and kurtosis methods resulting in poor estimation of the audio SNR. From Figures 3.7 and 3.9, we note that the RMS offset between the simulation and theoretical result is quite large in this case.

3. Finally when $\tau \gg T_c$ ($\tau_{norm} \gg 1$) and the channel has stationary characteristics, the PE/S and kurtosis methods provide a fairly good estimate of the audio SNR since the fading is averaged out. From Figures 3.8 and 3.11, we note that the RMS offset between the simulation and the theoretical result is low with the slope of all the curves roughly the same.

3.4 Laboratory Demonstration

We now compare these methods through a laboratory experiment, where all the system parameters are known and under our control. The experimental setup is shown in Figure 3.12. We generated an FM signal using an Agilent E4438C ESG vector signal generator by modulating a sinusoidal carrier at 453.2 MHz using a 123 Hz PL tone (no voice audio). In accordance with the TIA-603-B specifications for UHF band, given in Table 2.2, we set the maximum frequency deviation to 5 kHz. The signal generator is directly connected to a Tektronix RSA6114A spectrum analyzer. The spectrum analyzer has a "RF IQ vs. Time"

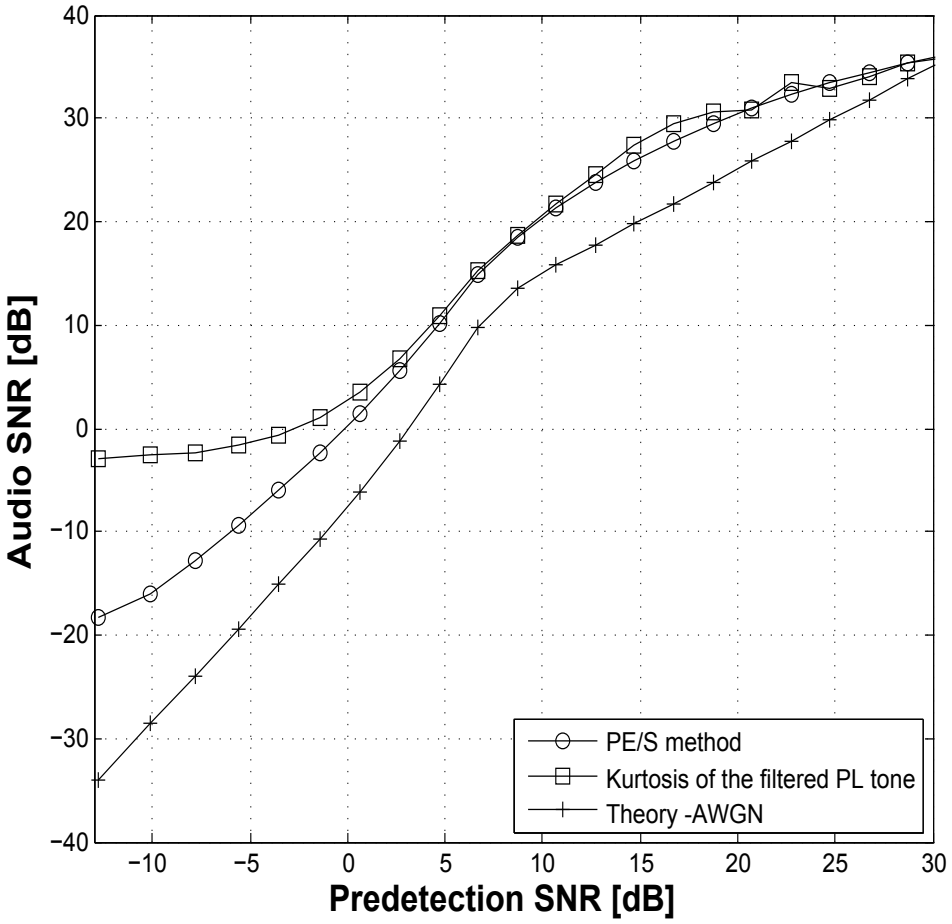

Figure 3.6: Relationship between audio SNR and predetection SNR. $\omega_{norm} \approx 0$, and $\tau_{norm} = 0.09$.

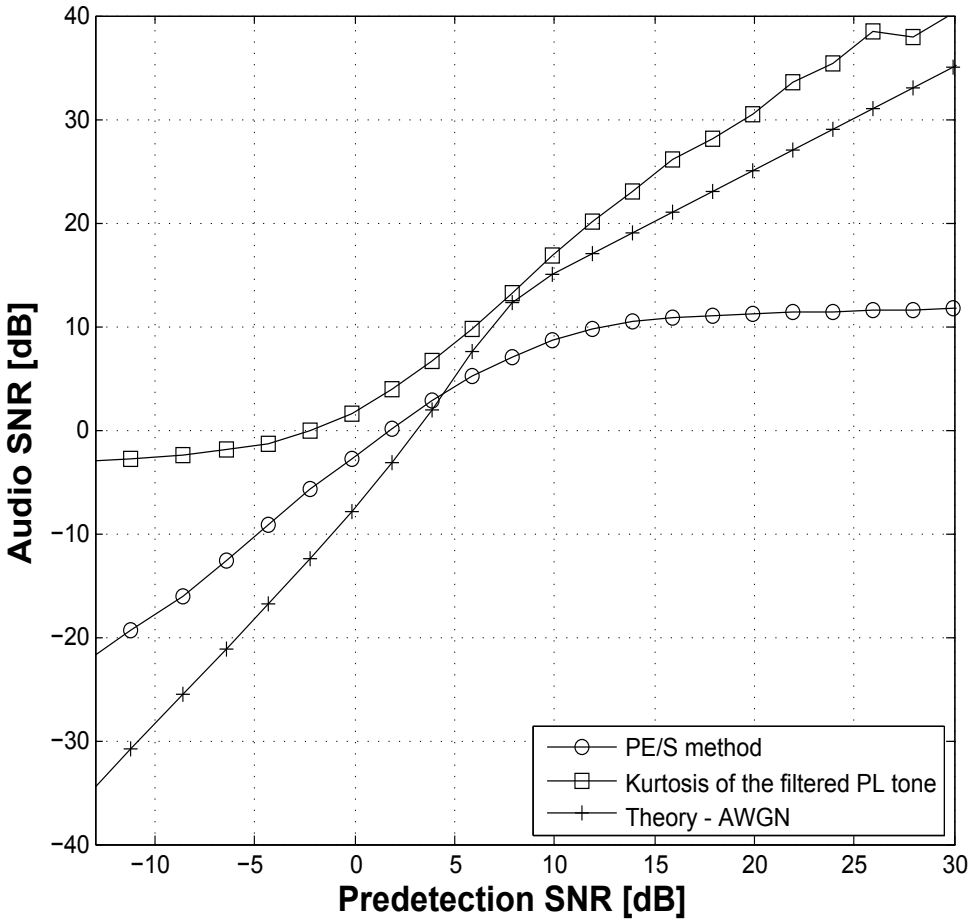

Figure 3.7: Relationship between audio SNR and predetection SNR. $\omega_{norm} \approx 0$, and $\tau_{norm} = 1$.

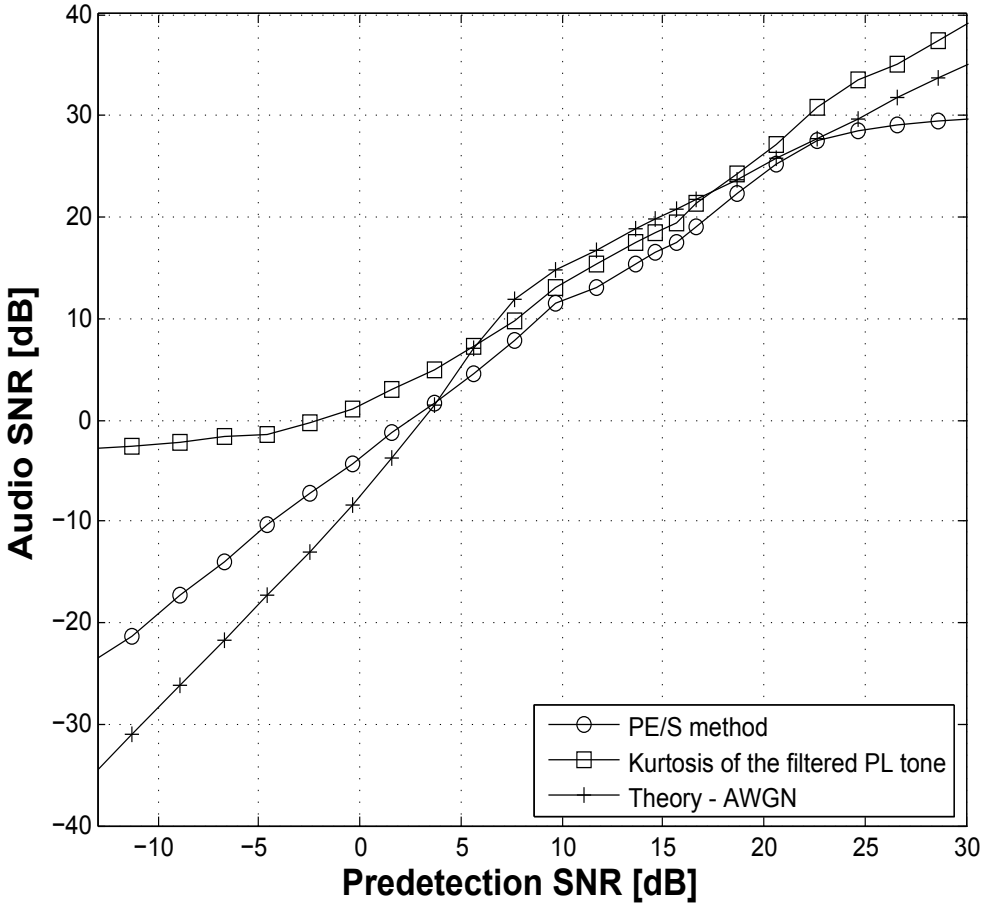

Figure 3.8: Relationship between audio SNR and predetection SNR. $\omega_{norm} \approx 0$, and $\tau_{norm} = 5$.

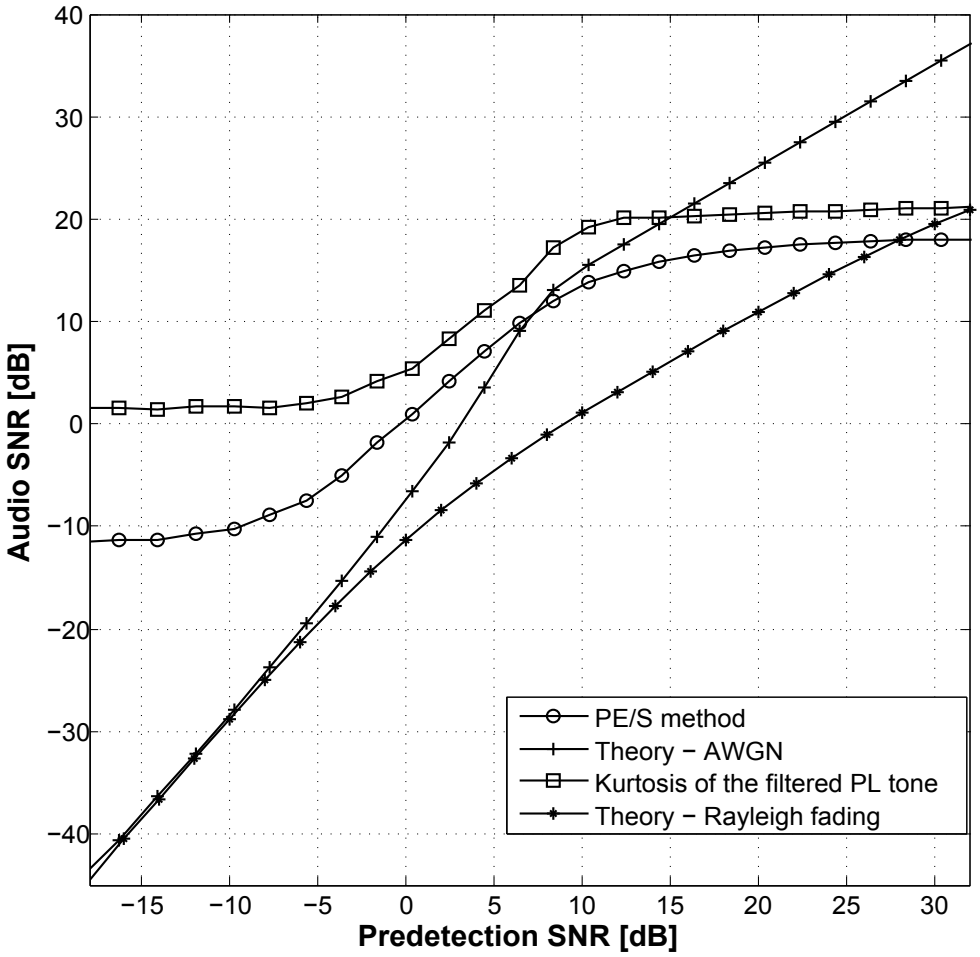

Figure 3.9: Relationship between audio SNR and predetection SNR. $\omega_{norm} = 1$, and $\tau_{norm} = 0.93$.

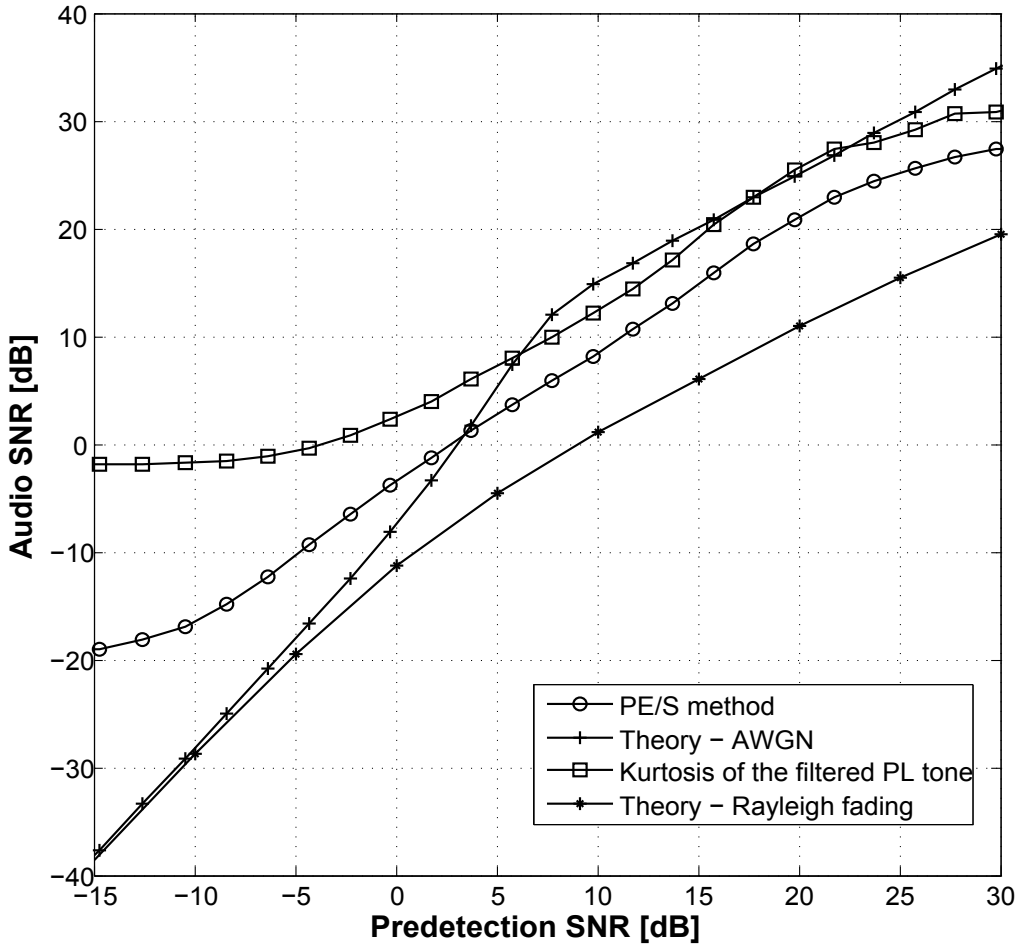

Figure 3.10: Relationship between audio SNR and predetection SNR. $\omega_{norm} = 1$, and $\tau_{norm} = 9.3$.

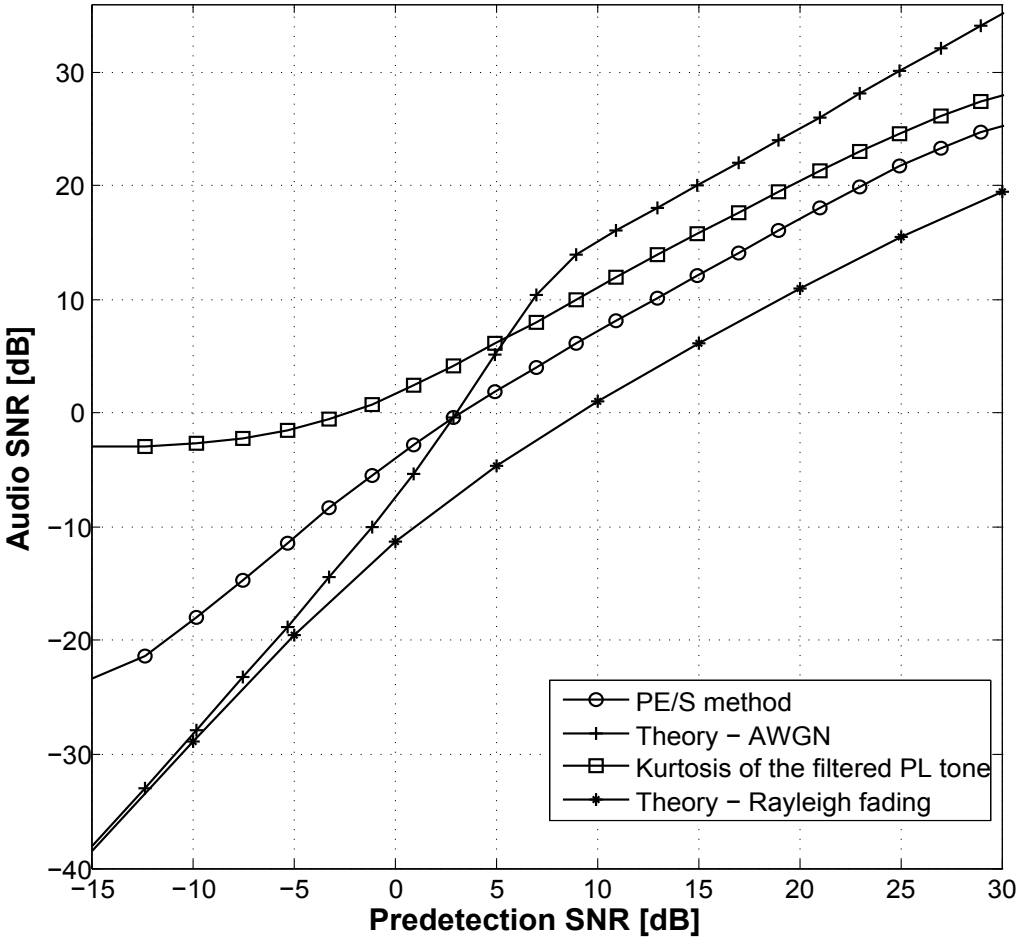

Figure 3.11: Relationship between audio SNR and predetection SNR. $\omega_{norm} = 1$, and $\tau_{norm} = 93$.

measurement option. We used this option to record the RF I and Q baseband data to a PC at a sampling rate of 781.25 ksps (which is greater than the Nyquist sampling rate). On the PC, we passed the recorded RF data through a Chebyshev FIR low-pass filter with 3-dB bandwidth set to 7.5 kHz. The order of the filter is 850 taps. We then measured the predetection SNR by measuring the total (signal+noise) power when the signal generator is on and the noise power when there is no transmission. The filtered RF signal is then demodulated using a FM detector which is same as in Section 2.2. The output of the detector is passed through an audio filter which is a Chebyshev FIR low-pass filter of order 803 taps and with 3-dB bandwidth (W) set to 3.5 kHz. The audio SNR is then measured using the PE/S method. The experiment is then repeated for different values of carrier power, to get a predetection SNR range from -12 dB to 35 dB.

Figure 3.13 shows the plot of the audio SNR as a function of predetection SNR using the simulations (PE/S and kurtosis methods) and the experimental result. Since the transmitter is directly connected to the receiver through a coaxial cable, the channel is stationary ($f_n = 0$). It was observed that on increasing the integration time (for the PE/S method) from 50 ms to 100 ms, the audio SNR increased by nearly 1.5 dB. Further increase in integration time from 100 ms to 200 ms resulted in quite small (about 0.2 dB) increase in audio SNR. So increasing integration time beyond 100 ms does not result in significant change in audio SNR. Hence a reasonable integration time would be 100 ms. We observe that the experimental result is in close agreement with the simulation (PE/S) result. Since the channel is stationary, we compare our result to Figure 3.5 and find that the results are similar.

We conclude that for a stationary channel both the PE/S and kurtosis methods give quite accurate results for predetection SNR between 5 dB and 25 dB.

3.5 Demonstration using Actual LMR Signal

We now compare these techniques using an actual LMR signal. We recorded an audio signal by tuning our ICOM IC-PCR1500 radio receiver to a local UHF-band police transmission. The average PSD of the received audio signal is shown earlier in Figure 2.2. It consists of the message signal and a PL tone at 162.2 Hz. The dynamic spectrum of the captured signal is also shown earlier in Figure 2.1. Table 3.2 lists the audio SNR computed using PE/S and kurtosis methods for different integration times. We observe that increasing the

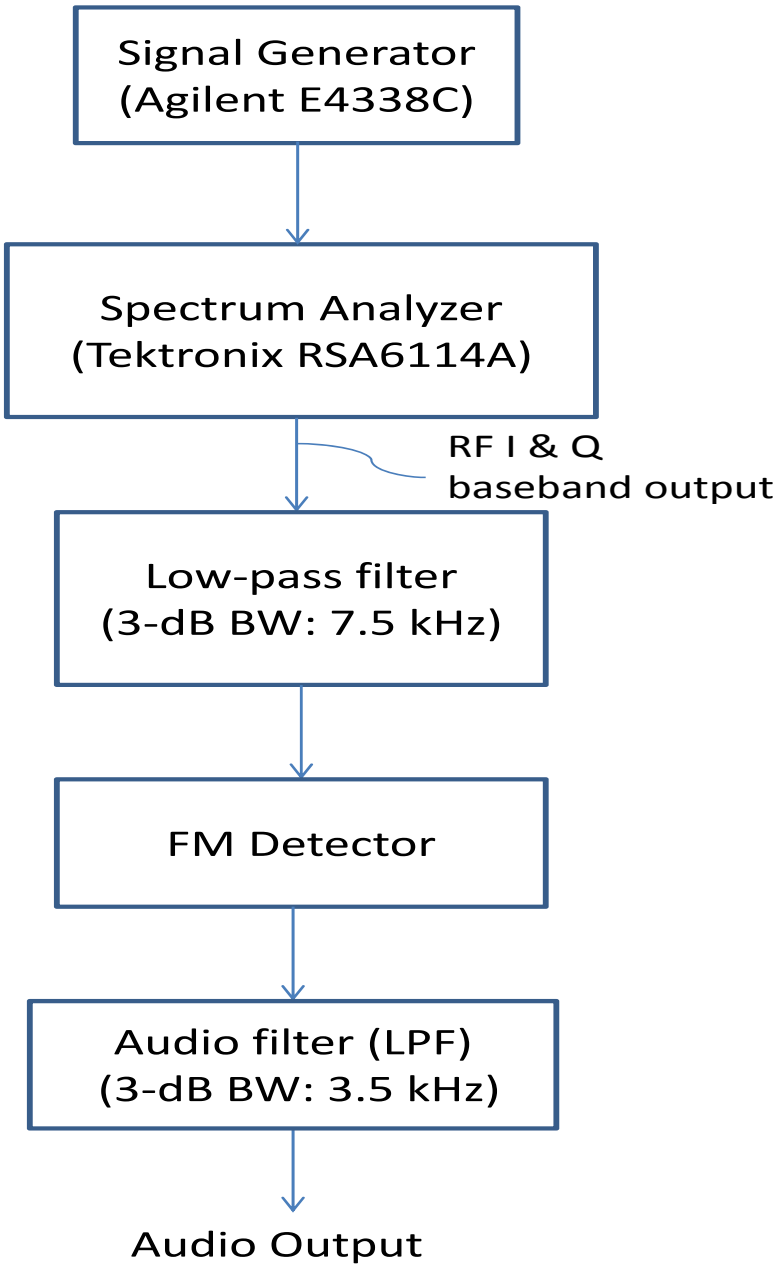

Figure 3.12: Control Experiment setup.

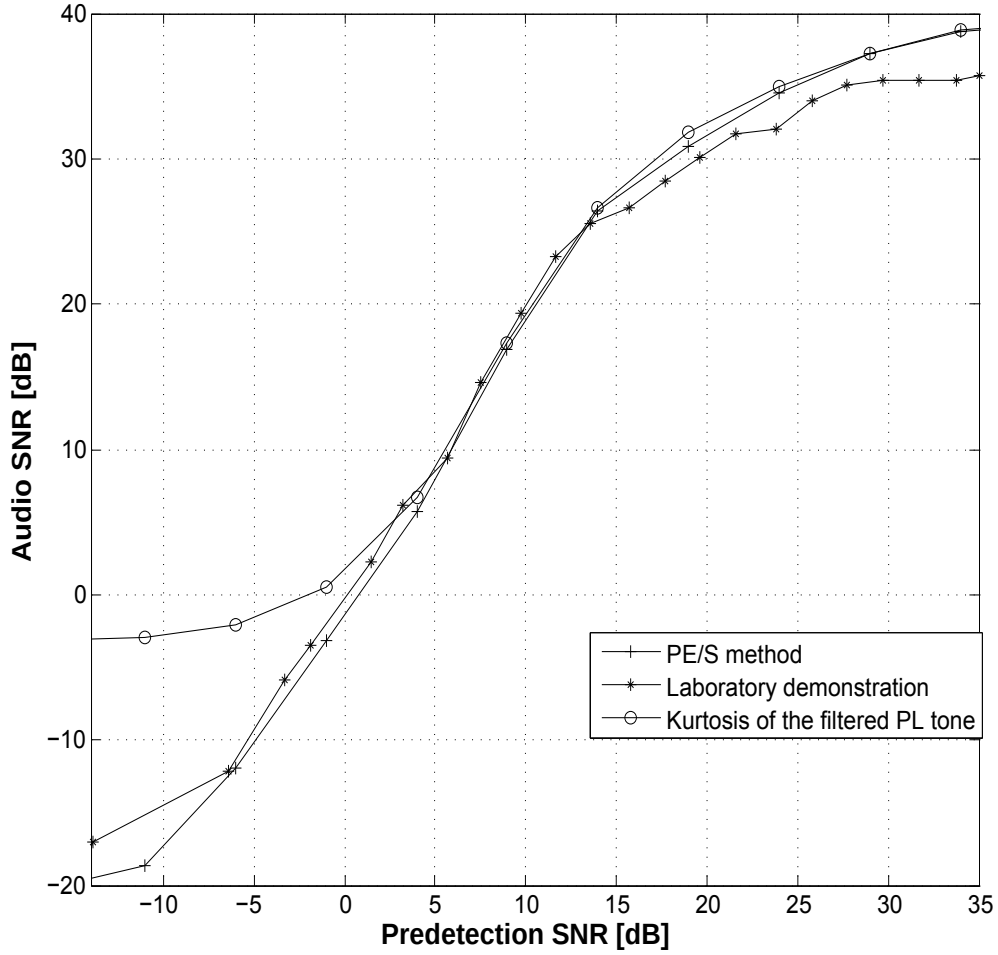

Figure 3.13: Relationship between audio SNR and predetection SNR using simulations and control experiment (Non-fading channel).

integration time from 50 ms to 100 ms increases the audio SNR by roughly 2 dB. However further increasing the integration time to 200 ms results in a dip of 1 dB. Hence a reasonable integration time for both the methods would be 100 ms. For 100 ms integration time, the PE/S and kurtosis methods give audio SNR values as 32.8 dB and 32.7 dB respectively. Referring to Figure 3.5, we observe that corresponding to our experimental audio SNR value, the simulation results for PE/S and kurtosis methods are fairly close. Since the experimental audio SNR values using PE/S and kurtosis method are also nearly equal, this establishes the validity of the PE/S and kurtosis methods.

3.6 Conclusions

From the simulation studies and experimental results, we conclude that under stationary channel conditions, the PE/S and kurtosis methods are in close agreement with each other for predetection SNR $>$ 5 dB and integration time within a few orders of magnitude of 100 ms. For SNR $<$ 5 dB, PE/S performs significantly better than kurtosis method. The offset between the two results increases with decreasing predetection SNR, and is roughly 14 dB at asymptotically low values of predetection SNR. Under fading conditions, it is observed that as the integration time is increased from a value much lower than the null-fading period to the null-fading period, the deviation of the PE/S and kurtosis results from the theoretical result increases by few dB. However on making the integration time much larger than the null-fading period, the deviation actually decreases as the fading behavior get averaged out. In general, at low SNR values, the kurtosis result flattens out earlier than the PE/S curve. This is related to the fact that PE/S is statistically optimum where as kurtosis is not.

We conclude that it is possible to estimate FM audio quality from PL tone analysis over a wide range of commonly encountered conditions.

Table 3.2: Effect of integration time on the performance of PE/S and kurtosis methods as applied to an actual LMR signal.

Integration time τ	Audio SNR	
	PE/S method	Kurtosis method
50 ms	30.9 dB	30.7 dB
100 ms	32.8 dB	32.7 dB
200 ms	31.6 dB	31.3 dB

Chapter 4

Estimation of Predetection SNR from Audio SNR

The scheme described in Section 1.2 (Figure 1.1), using the approach described in Chapter 3, makes it possible to compare the performance of LMR antennas on the basis of audio SNR. The final step in the scheme in Figure 1.1 involves measuring and comparing the predetection (RF) SNR of the antennas, which is the topic of this chapter. A theoretical relationship between audio SNR and predetection SNR was worked out in Sections 2.3 and 2.4.2. Figures 2.6 and 2.7 show the estimated predetection SNR as a function of audio SNR for an AWGN channel and a Rayleigh fading channel respectively. We now consider the viability of using these results to estimate predetection SNR from audio SNR. For this we study the accuracy of the predetection SNR determined in this manner by comparing it with the simulation and experimental predetection SNR in Sections 4.1 and 4.2 respectively. Finally, in Section 4.3 ("Conclusions"), we conclude the chapter with comments on the limitations and accuracy of theoretical method. We also consider the range of predetection SNR over which the method works satisfactorily.

4.1 Performance for Simulated Signals (No Fading)

In this section, we evaluate the accuracy of the theoretical method described in Section 2.3 using simulations. The channel is assumed to be additive white Gaussian noise (AWGN) with no fading. The FM detector is implemented as a sequence of DSP operations as described

in Section 2.2. The audio SNR is determined using PE/S evaluation of the PL tone. For a stationary channel, increasing the integration time beyond 100 ms does not have any significant impact on the performance of the PE/S method (Section 3.3.2). Therefore, we set the integration time to 100 ms. B and W are set to 17 kHz and 3.5 kHz respectively.

The theoretical predetection SNR estimate and the measured predetection SNR are plotted against the audio SNR in Figure 4.1. We observe that the results are consistent but not in close agreement. The theoretical result follows the measured predetection SNR with a 1–10 dB offset, for audio SNR range from -15 dB to 35 dB. Some offset should be expected because there are some approximations and assumptions in the theoretical result. Hence we perform an experiment as described in the next section to determine the validity of the results.

4.2 Laboratory Evaluation

In this section, we evaluate the accuracy of the theoretical predetection SNR estimation method (Section 2.3) first through a series of reference experiments and then using signals received from actual LMR transmitters. The two reference experiments differ in their implementations of the FM detector. Reference experiment 1 uses the same FM detector as the one used in simulations (in Section 4.1) whereas reference experiment 2 replaces the simulation receiver with a hardware (ICOM IC-PCR 1500) receiver.

4.2.1 Reference Experiment 1

We now compare the theoretical method with measurements from a reference experiment, where all the system parameters are known and under our control. The experimental setup is shown in Figure 3.12. We generated an FM signal using Agilent E4438C ESG vector signal generator by modulating a sinusoidal carrier at 453.2 MHz using a 123 Hz PL tone (no voice audio). The maximum frequency deviation is set to 4 kHz. The signal generator is directly connected to Tektronix RSA6114A spectrum analyzer. The spectrum analyzer has a "RF IQ vs. Time" measurement option. We used this option to record the RF I and Q baseband data to a PC. On the PC, we passed the recorded RF data through a Chebyshev FIR low-pass filter with 3-dB bandwidth ($B/2$) set to 7.5 kHz. The order of the filter is 850 taps.

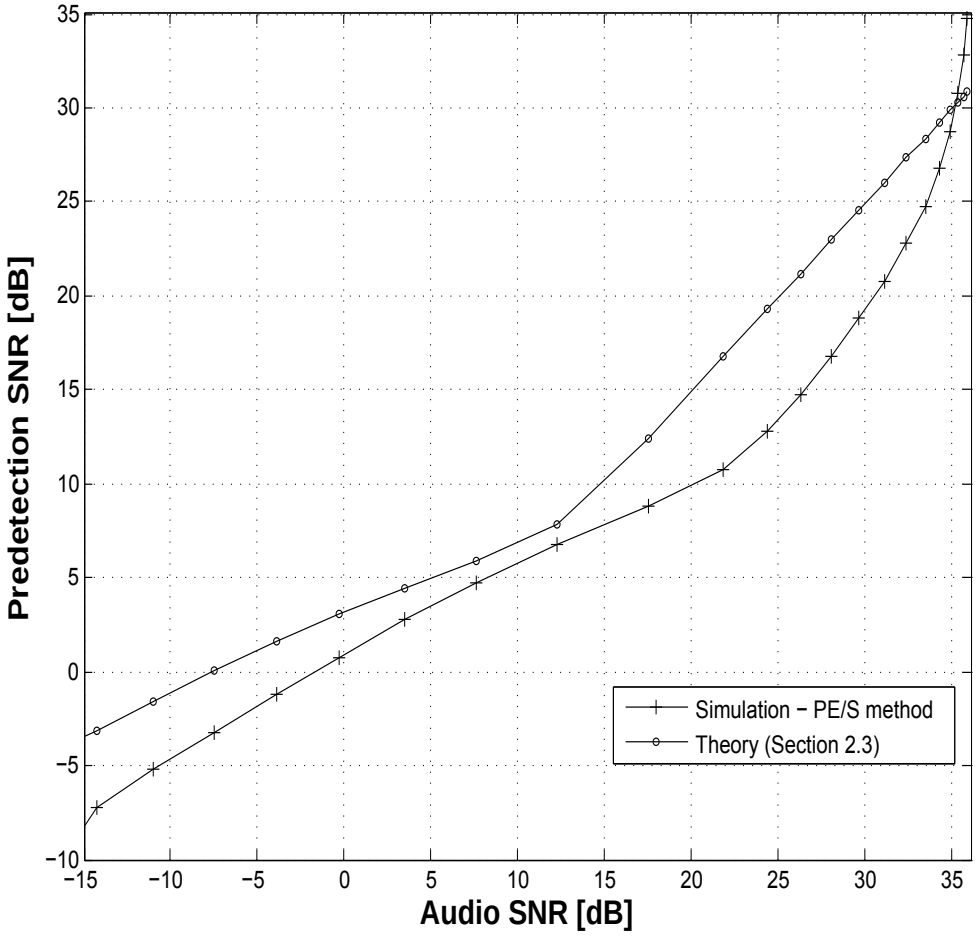

Figure 4.1: Relationship between predetection SNR and audio SNR (Non-fading channel).

We then measured the predetection SNR by measuring the total (signal+noise) power when the signal generator is on and the noise power when there is no transmission. The filtered RF signal is then demodulated using a FM detector which is same as in Section 2.2. The output of the detector is passed through an audio filter which is a Chebyshev FIR low-pass filter of order 803 taps and with 3-dB bandwidth (W) set to 3.5 kHz. The audio SNR is then measured using the PE/S method. The integration time for the PE/S method is set to 100 ms. The experiment is then repeated for different values of carrier power, to get a predetection SNR range from -7 dB to 35 dB.

Figure 4.2 shows predetection SNR as a function of audio SNR, using the experimental result, the simulation, and the theoretical result. We observe that the experimental result is in close agreement with the simulation result. This is not surprising since the reference experiment is different from the simulation only in that the simulation modulator is replaced by a hardware modulator. Thus agreement between the simulation and the reference experiment indicates only that the modulator is not the source of the disagreement between simulation and reference experiment in Figure 4.1 noted in Section 4.1. Hence, in the next section, we perform another reference experiment which replaces the simulation receiver with a hardware receiver.

4.2.2 Reference Experiment 2

We now compare the theoretical method with measurements from an another reference experiment. The experimental setup is shown in Figure 4.3. We generated an FM signal as described in Section 4.2.1. The signal generator output is split two ways using a Mini-Circuits ZFSC-2-2500+ power splitter. One of the outputs goes to a Tektronix RSA6114A spectrum analyzer while the other goes to a ICOM IC-PCR 1500 receiver. The output from the spectrum analyzer is then used to measure the predetection SNR as described in Section 4.2.1. The audio output from the ICOM receiver is recorded to a PC. On the PC, we filter the recorded audio through a Chebyshev FIR low-pass filter of order 1003 taps and with 3-dB bandwidth (W) set to 3.5 kHz. The audio SNR is then measured using the PE/S method. The integration time for the PE/S method is 100 ms. The experiment is then repeated for different values of carrier power to get a predetection SNR range from -12 dB to $+25$ dB.

Figure 4.4 shows predetection SNR as a function of audio SNR, using the experimental result,

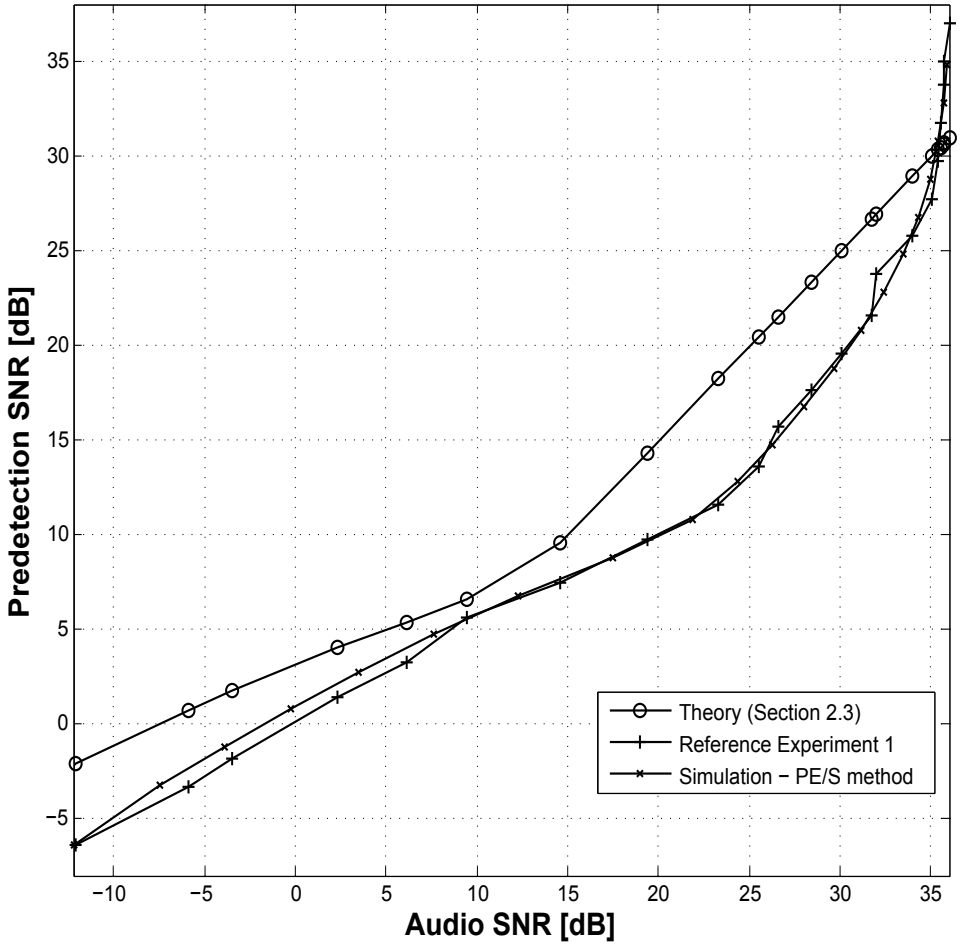

Figure 4.2: Reference Experiment 1 - Relationship between predetection SNR and audio SNR.

the simulation, and the theoretical result. We observe that the experimental result is in close agreement with the simulation result for audio SNR between 0 dB and 20 dB. For audio SNR < 0 dB, there is a 1–3 dB difference between the simulation and experimental result. For audio SNR > 20 dB, the difference between the simulation and experimental results increases and becomes asymptotically large at audio SNR of 25 dB. This is the expected behavior. Due to the non-linear nature of FM modulation, the SNR at the output of the FM detector doesn't get any better by increasing the predetection SNR beyond a particular value. In order to make our results from reference experiment 2 more conclusive, in the next section we perform another experiment where we capture signals received from the actual LMR transmitters.

4.2.3 Demonstration Using Actual LMR Signals

In this section, we determine the relationship between the RF SNR and the audio SNR for signals received from actual LMR transmitters and find out how it compares with the theoretical result and simulations considered in previous sections. The experimental setup is shown in Figure 4.5. The received signal from the antenna is first passed through a series combination of Agilent HP 8494A and 8495B manual step attenuators and then split two ways using a Mini-Circuits ZFSC-2-2500+ power splitter. The rest of the signal processing is same as in reference Experiment 2. Both the Tektronix RSA6114A spectrum analyzer and the ICOM IC-PCR1500 radio receiver are tuned to a local LMR transmission (Blacksburg Transit bus service) at 453.625 MHz with a PL tone at 203.5 Hz. B and W are set to 15 kHz and 3.5 kHz respectively. The audio SNR is measured using the PE/S method. The integration time for the PE/S method is set to 100 ms. The experiment is repeated for different values of external attenuation to get a predetection SNR range from -12 dB to $+25$ dB.

The main objective of doing this experiment was to evaluate the accuracy of the theoretical method (Section 2.3) for the actual LMR signals and use the results obtained thereof as a reference for the field experiments to be done later (described in Chapter 5). Figure 4.6 shows predetection SNR as a function of audio SNR, using the experimental result, the simulation, and the theoretical result. The results are similar to those observed in reference Experiment 2. We observe that the experimental result is in close agreement with the simulation result for audio SNR between 3 dB and 36 dB. For audio SNR < 0 dB, there is a 1–3 dB difference

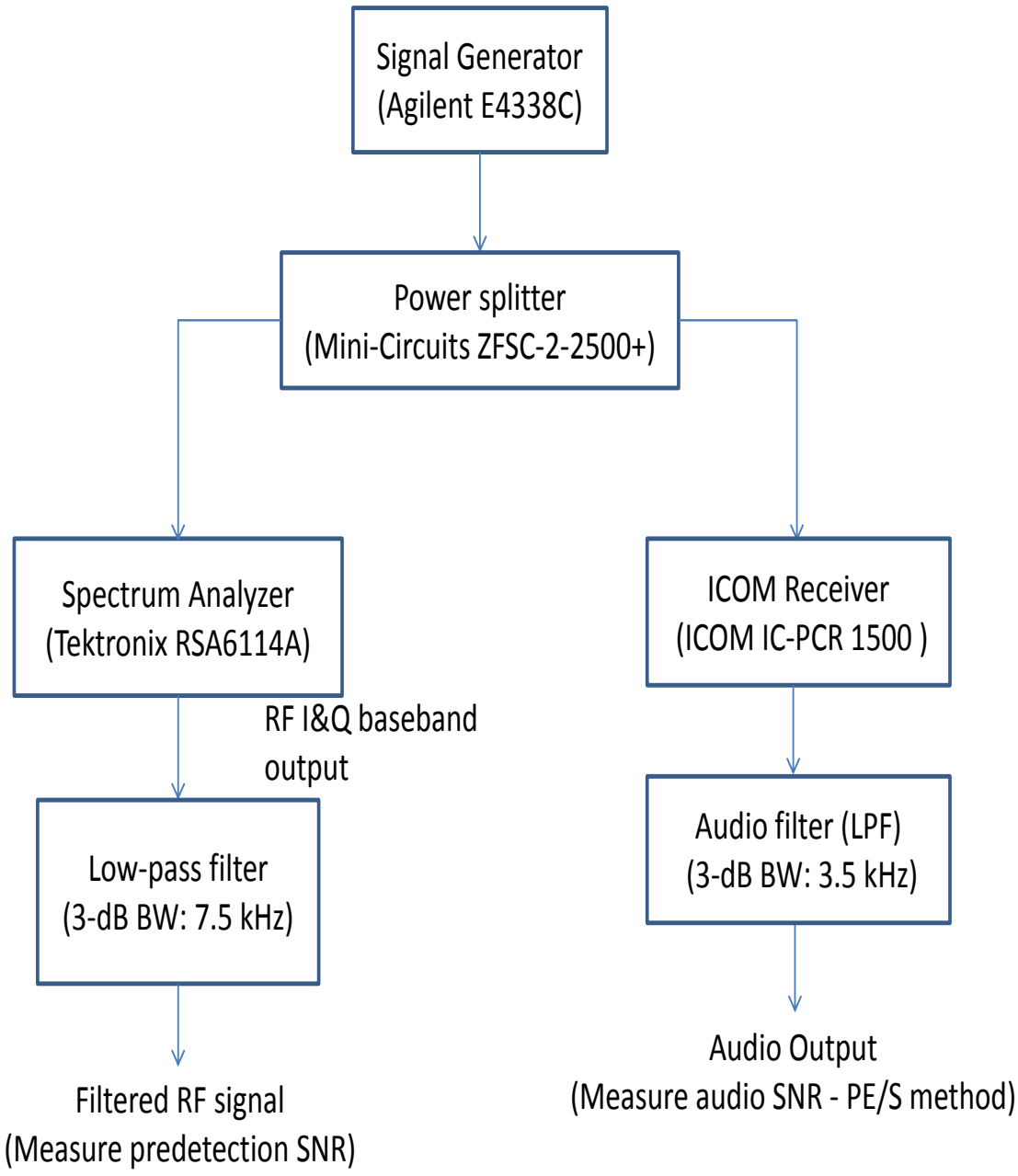

Figure 4.3: Reference Experiment 2 setup.

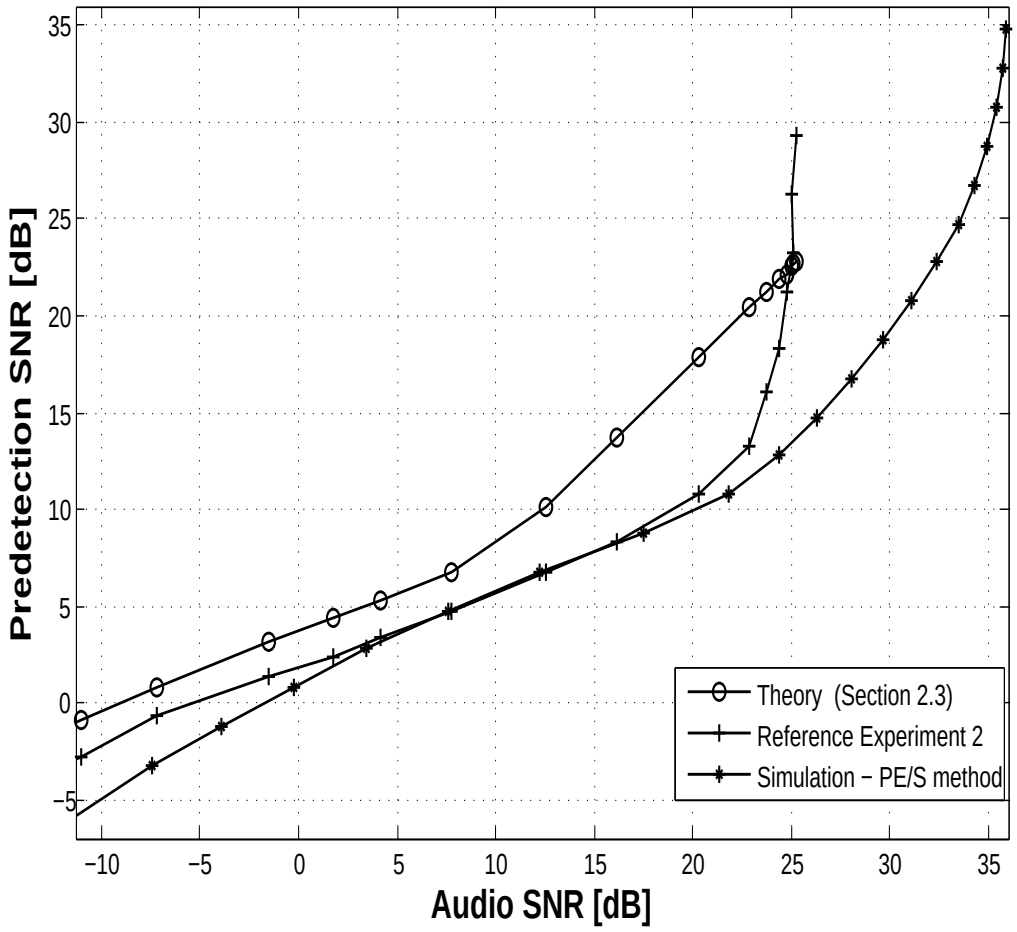

Figure 4.4: Reference Experiment 2 - Relationship between predetection SNR and audio SNR.

between the simulation and experimental result.

4.3 Conclusions

Our procedure for estimating predetection SNR from audio SNR is as follows. Measure the audio SNR by following the procedure described in Section 4.2.2. Then use the theoretical result described in Section 2.3 to estimate the predetection SNR from the audio SNR. If desired, the accuracy of the result can be further improved by accounting for the relatively constant difference between theoretical and experimental/simulation results seen in Figure 4.6.

The resulting estimated predetection SNR is quite accurate (within 0.5 dB of actual result) for predetection SNR between +3 dB and +36 dB. For predetection SNR less than +3 dB, there is a 1–3 dB difference between the estimated and actual value of predetection SNR. We conclude that our proposed method works with ±3 dB accuracy for predetection SNR between −6 dB and +36 dB.

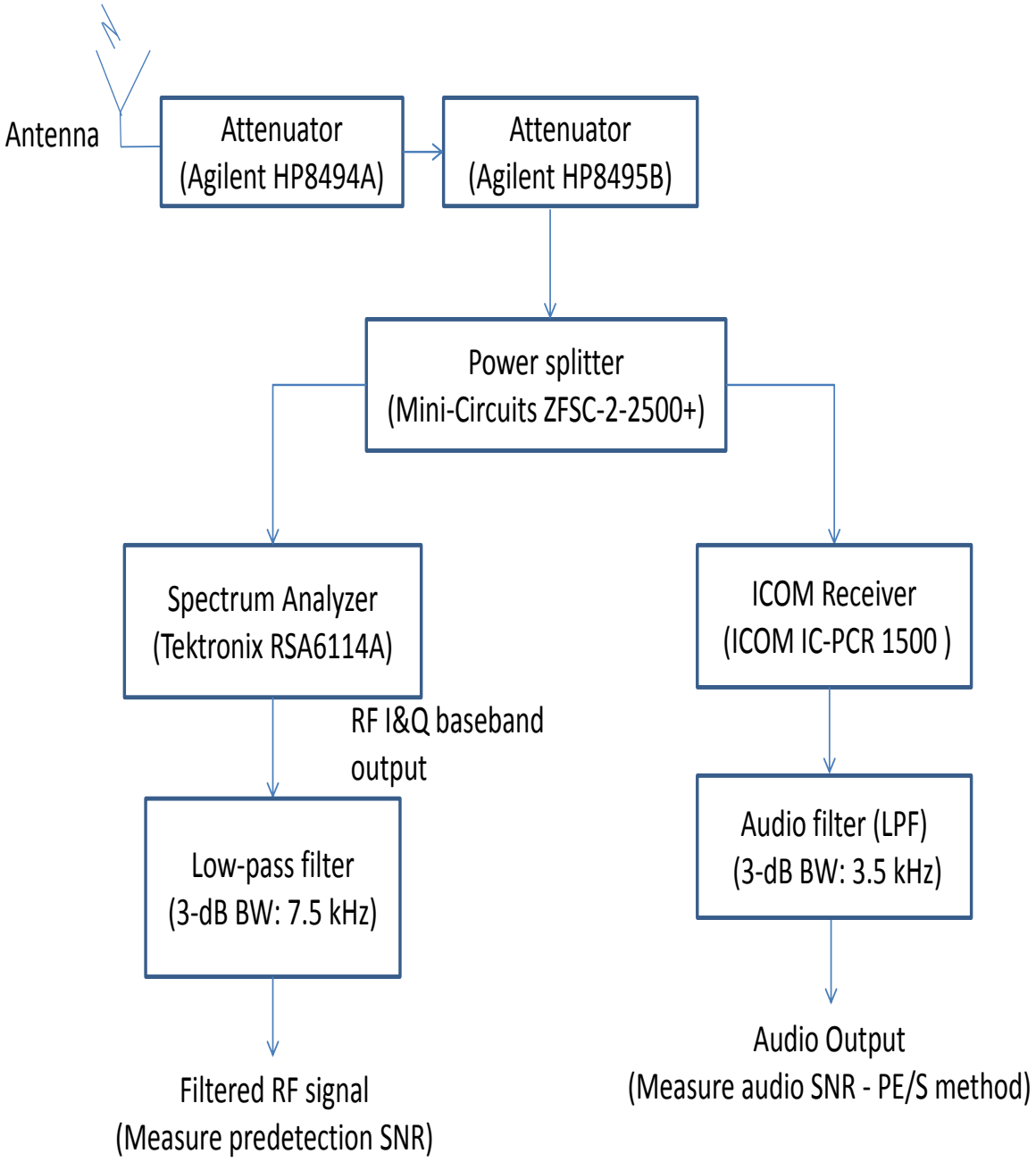

Figure 4.5: Setup for capturing actual LMR signals.

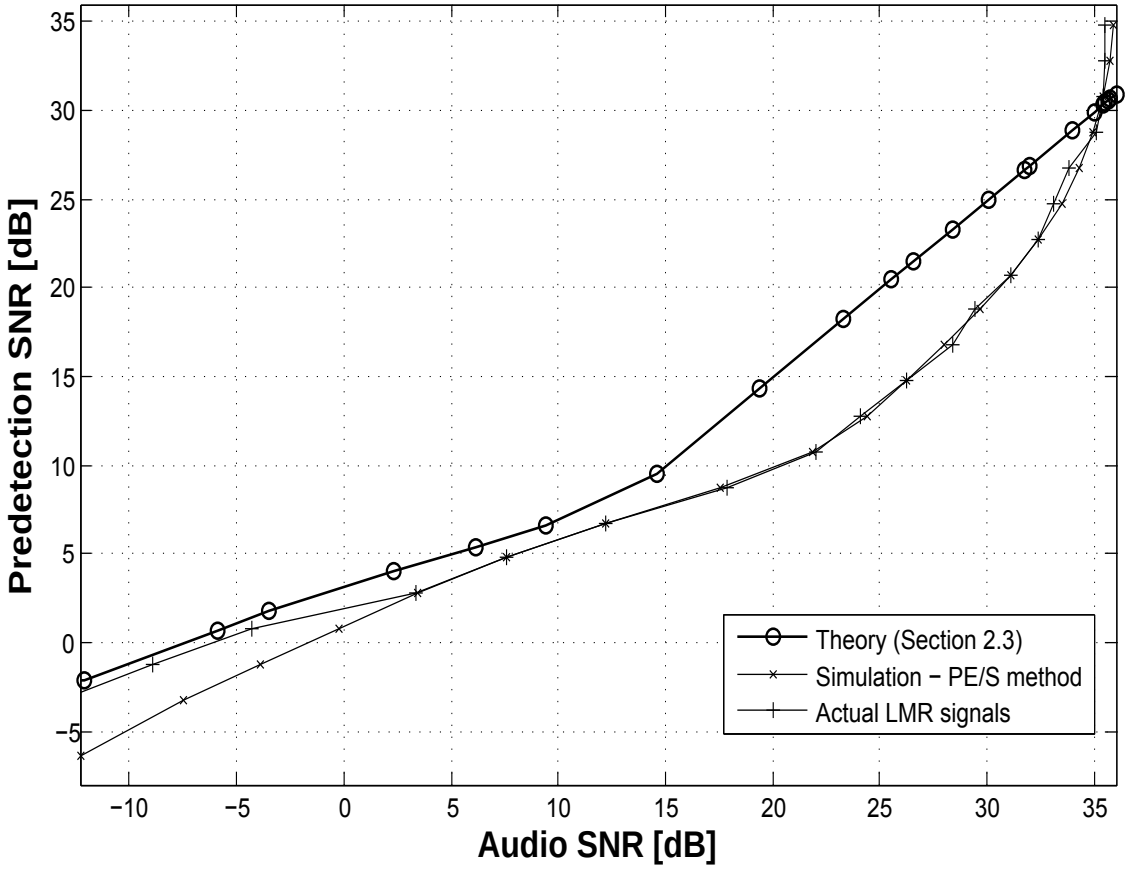

Figure 4.6: Relationship between predetection SNR and audio SNR for signals received from actual LMR transmitters.

Chapter 5

Field Evaluation of the LMR Multiband Antenna System

In this chapter, we present an application of the methodology developed in previous chapters: A comparison of a prototype LMR multiband antenna system to that of a commercial antenna. The prototype antenna system was developed as a part of the project "Antenna Systems for Multiband Mobile & Portable Radio" [4]. Section 5.1 ("Summary") provides a brief overview of this experimental evaluation. The experimental setup is described in Section 5.2 ("Experimental Setup and Measurements"). For each of the frequency bands of interest, the performance of the prototype antenna system is compared to that of a commercial antenna using an analysis of signals received from actual LMR transmitters. Section 5.3 ("Signal Processing") presents the procedure for analyzing the received signals to determine the audio and RF SNRs. The results are summarized in Section 5.4 ("Results").

5.1 Summary

The goal of this evaluation was to demonstrate an experimental LMR antenna which can operate in the VHF-Low (25–50 MHz), VHF-High (138–174 MHz), 220–222 MHz, UHF (406–512 MHz), and 764–862 MHz bands without physically swapping antennas. The experimental antenna system consists of a reconfigurable monopole-type antenna consisting of a base antenna plus a switched extension element with an automatic electronic antenna tuner, and is documented in [19]. Preliminary field measurements using the antenna with a rudimentary

version of the antenna tuner are reported in [20]. In this chapter, we present a more thorough evaluation using a completed implementation of the antenna tuner in the VHF-High, UHF, and 800 MHz bands. In each band the performance of the prototype antenna system is compared to that of a commercial antenna using the method described in previous chapters, summarized by Figure 1.1. The VHF-Low and the 220 MHz bands are however not locally available for testing in this manner, and so are not included in this testing.

5.2 Experimental Setup and Measurements

Figure 5.1 shows the block diagram of the experimental setup and Figure 5.2 shows photographs of the test rig taken from different viewing angles. The prototype electronically-reconfigurable monopole antenna has a total length of 1.4 m including a 3.2 mm diameter electronically-switchable extension. The commercial (reference) antenna and the reconfigurable antenna are mounted on their own individual ground planes, each about 1.2 m x 0.6 m in size. The ground planes are mounted to the top of a cart, which carries all other instrumentation (including, in the case of reconfigurable antenna, the antenna tuner) on a lower shelf. For both systems, the ICOM IC-PCR1500 receivers and the antenna terminals are connected by a total of about 6 ft of semi-rigid 50 Ω coaxial cable. Also, variable attenuators are inserted at the input of both the receivers in order to lower the audio SNR to values in the 5–35 dB range, where small differences in antenna system performance result in relatively large differences in audio SNR. Specifically, a series combination of step attenuators (Agilent HP8494A and HP8495B) is used for the reconfigurable antenna system, and a dual concentric rotary attenuator (JFW 50DR-061-SMA) is used for the commercial antenna system. Based on initial trials, we found out that reasonable attenuation values were 25 dB for VHF-High, 26 dB for UHF, and 23 dB for 800 MHz measurements. The ICOM receivers are connected to identical but separate netbook-type computers. The control software on the PCs is used to tune the ICOM receiver to desired receiver settings and capture audio. The captured audio signals then undergo signal processing as described in Section 5.3 to yield the audio and RF SNRs.

All measurements reported in this chapter were performed on the third floor balcony of Whittemore Hall, on the main (Blacksburg, VA) campus of Virginia Tech. The cart shown in Figure 5.2 was periodically reoriented to mitigate against systematic bias from multipath fading. The measurements in each orientation as well as the the results for the combined set

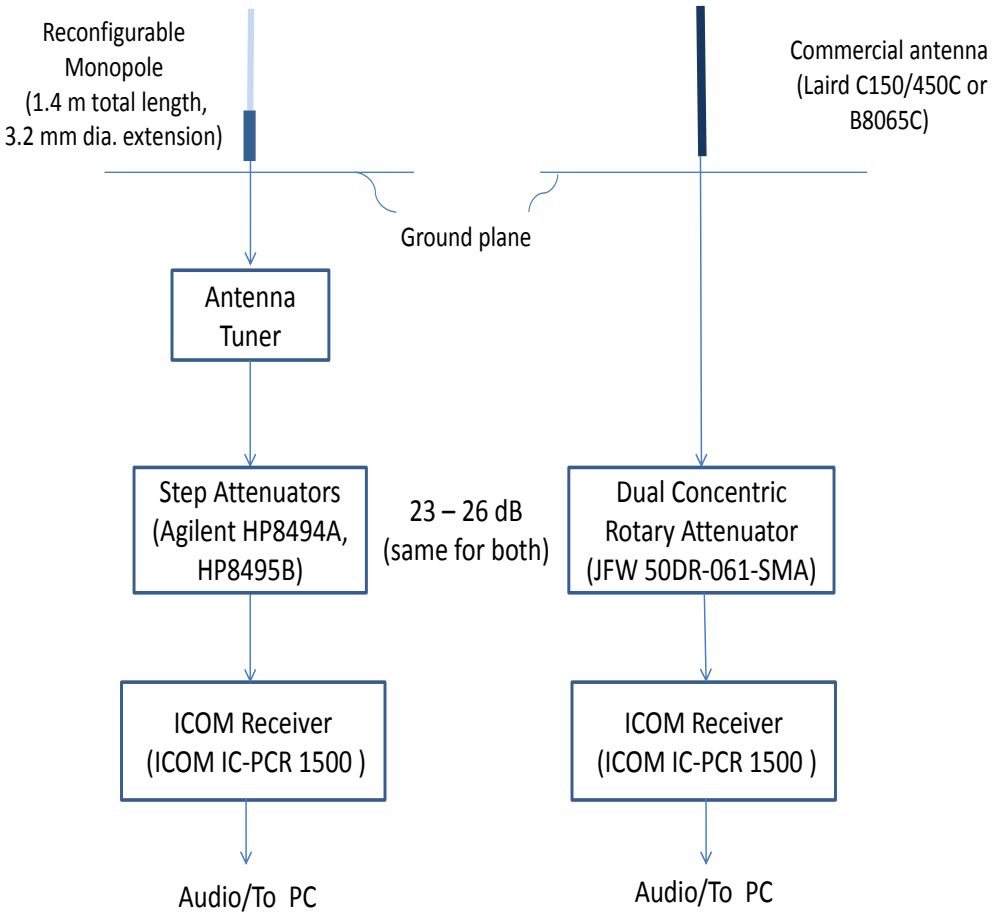

Figure 5.1: Block diagram of the field setup.

Figure 5.2: Location and test fixture. The reconfigurable antenna and the commercial antenna (in this case Laird Tech. Model C150/450C) appear to the left and right, respectively, in two figures. The automatic electronic tuner is the aluminium box located directly under the reconfigurable antenna. Views are *top/left*, approximately Southwest; *top/right*, approximately Northwest; *bottom/left*, approximately South; *bottom/right*, approximately North.

of orientations is reported in each case.

Table 5.1 shows the specific LMR systems that were monitored to collect data for this study. Also indicated is the commercial antenna which was used in each case. The Laird Tech. Model C150/450C is a dual-band antenna marketed for use in the 150–174 MHz and 450–474 MHz bands, whereas the Laird Tech. Model B8065C is a single band antenna marketed for use in the 806–896 MHz band. Additional information on the performance of these commercial antennas can be found in [20] (see especially Figures 1 and 3) as well as [21].

5.3 Signal Processing

For each separate and identifiable transmission recorded, the corresponding segments of the audio signal from both the prototype antenna and the commercial antenna are first passed through a Chebyshev FIR low-pass filter of order 1607 and with 3-dB bandwidth set to 270 Hz. This filters out the voice component of the message signal leaving behind the PL tone and the sub-audio noise. Then the SNR of the PL tone is determined using the PE/S method, as described in Section 3.1. The integration time for the PE/S method is set to 100 ms. Having determined the audio SNR, we estimate the RF SNR for each transmission using the procedure presented in Section 4.3. The relative performance of these antennas was then determined by comparison of the audio SNRs and RF SNRs accumulated over many transmissions, as shown in Figures 5.3–5.8.

5.4 Results

In this section, we present a comparative analysis of the audio SNR and RF SNR results for both the antennas for different test rig orientations. Sections 5.4.1, 5.4.2, and 5.4.3 present the results for the VHF-High, UHF, and 850 MHz bands respectively.

5.4.1 VHF High – 155.535 MHz

Figure 5.3 shows the estimated audio SNR for each transmission simultaneously received by both the antenna under test (the reconfigurable antenna system) and the reference (com-

Table 5.1: LMR systems and commercial antennas used for testing in each band.

Band	Freq. (MHz)	PL (Hz)	System/User	Commercial Antenna
VHF-High	155.535	162.2	VT Police	Laird Tech. C150/450C
UHF	453.625	203.5	Blacksburg Transit	Laird Tech. C150/450C
800 MHz	851.150	186.2	Blacksburg Police	Laird Tech. B8065C

mercial) antenna indicated in Table 5.1. In this representation, each point of the scatter plot represents a transmission, and the vertical and horizontal coordinates are the observed audio SNRs obtained from the reconfigurable antenna and the commercial antenna, respectively. Therefore the data points above or below the diagonal line indicate that the reconfigurable antenna is performing better or worse, respectively, than the commercial antenna. We also note that there is a significant amount of scatter in results; this can be attributed to the time-varying nature of multipath fading, which can be expected to have similar characteristics everywhere and underscores the importance of using multiple orientations of the test fixture as explained in Section 5.2.

A statistical analysis of the audio SNR data is also presented in Table 5.2. We find that the result using all data from both the orientations ("Combined") shows that the reconfigurable antenna is, on an average, +0.3 dB better, with a correlation coefficient $r = +0.43$. The time-varying multipath conditions results in rather large standard deviation in the ratio of audio SNRs. This is further corroborated by the observation that there is a large difference in the performance between the two orientations; indicating that one of the two possible antenna positions is significantly better than the other.

Figure 5.4 shows the estimated RF SNR (in dB) in a manner similar to the audio SNR result described in Figure 5.3. A statistical analysis of the RF SNR data is presented in Table 5.3. We find that the "Combined" result shows that the reconfigurable antenna is, on an average, +0.1 dB better, than the commercial antenna. As expected from the theory (and also Section 2.3), the standard deviation in the result is smaller than that in the audio SNR results.

We conclude that the reconfigurable antenna is certainly better than the commercial antenna on a statistical basis, and perhaps is also consistently better, although the later is difficult to ascertain since it is obviously impossible to evaluate both the antennas simultaneously at the same location.

5.4.2 UHF – 453.625 MHz

The audio SNR results for the 453.625 MHz testing are shown in Figure 5.5 in the same manner as for 155.535 MHz testing described above. Table 5.4 presents the statistical analysis of this data. We note that the "Combined" result indicates that the reconfigurable antenna is, on an average, +3.5 dB better, with a correlation coefficient $r = +0.69$, and with a much smaller standard deviation than the VHF-High measurements. We also note once again that one of the orientations is statistically better than the other.

From Figure 5.6 and Table 5.5, we note that this corresponds to an RF SNR difference of about 1.2 dB between the two antenna systems. We conclude that the reconfigurable antenna system is performing significantly better than the commercial antenna at 453.625 MHz.

5.4.3 851.150 MHz

The audio SNR results for the 851.150 MHz testing are shown in Figure 5.7 in the same manner as for 155.535 MHz and 453.625 MHz testing described above. Table 5.6 presents the statistical analysis of this data. We note that the "Combined" result indicates that the reconfigurable antenna is, on an average, about 2.6 dB worse than the commercial antenna. From Figure 5.8 and Table 5.7, we note that this corresponds to an overall RF SNR difference of 1.1 dB between the two antenna systems.

We have identified two possible reasons for the relatively poor performance in this band. One possible reason is the insertion loss from the directional couplers used in the "tuner board" of the tuner in the reconfigurable antenna system. The insertion loss is significantly worse in the 800 MHz band than at lower frequencies [19]. Also since the closed-loop tuning [19] was disabled for this test, another reason for poor performance could be that the tuning solution was not optimally set. Either reason would be consistent with our previous finding that the reconfigurable antenna + rudimentary tuner (stubline-only) system evaluated in [20] exhibited audio SNR performance comparable to the same commercial antenna used in the study in this band. Thus, we believe that simple adjustments to the reconfigurable antenna system would be sufficient to realize the same relative level of performance in 800 MHz band as is exhibited in the VHF-High and UHF bands.

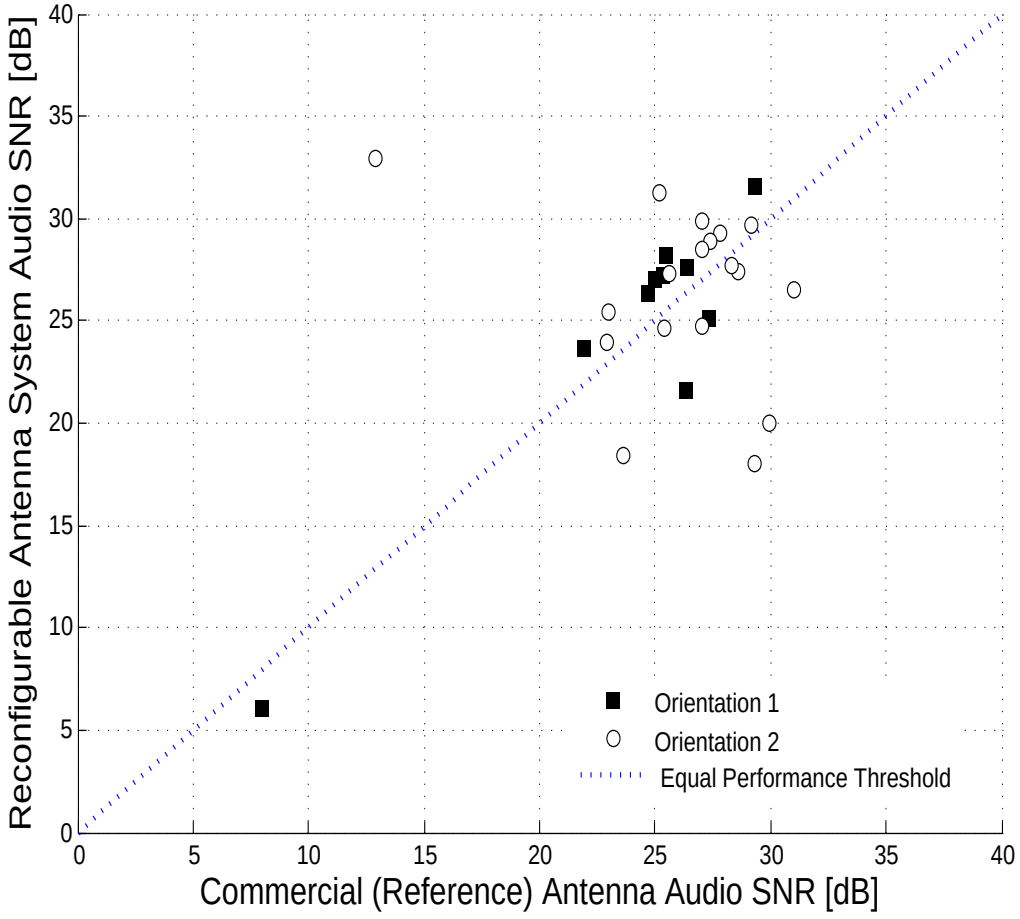

Figure 5.3: 155.535 MHz: Estimated audio SNR for each transmission simultaneously received by both the reconfigurable antenna system and the commercial antenna.

Table 5.2: Statistical analysis of the data in Figure 5.3. x and y correspond to the measured audio SNRs, in dB, for the commercial antenna and reconfigurable antenna system respectively. So "mean$(y-x)$" is positive when the reconfigurable antenna is better. "std$(y-x)$" is the standard deviation of $y-x$. r is the correlation coefficient between y and x.

Orientation	No. Transmissions	mean$(y-x)$	std$(y-x)$	r
1	10	+0.5 dB	2.5 dB	+0.94
2	18	+0.2 dB	6.6 dB	−0.28
Combined	28	+0.3 dB	5.4 dB	+0.43

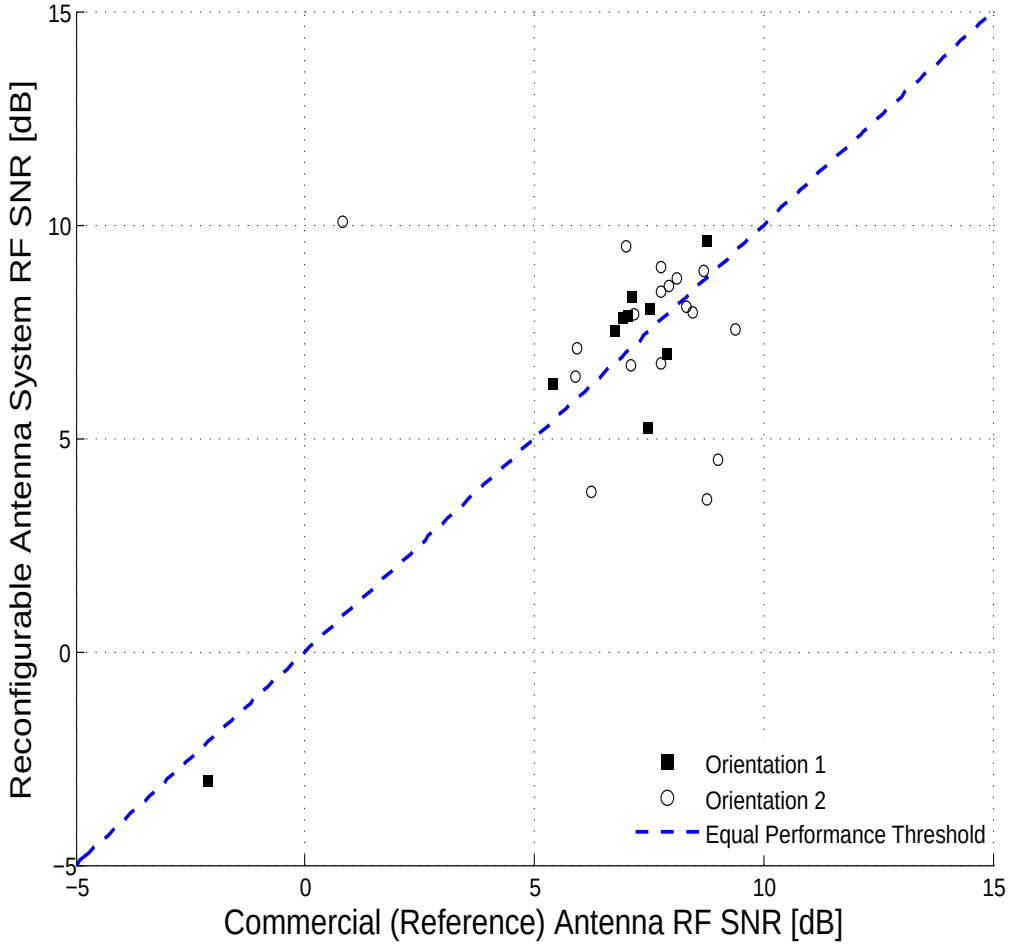

Figure 5.4: 155.535 MHz: Estimated RF SNR for each transmission simultaneously received by both the reconfigurable antenna system and the commercial antenna.

Table 5.3: Statistical analysis of the data in Figure 5.4. x and y correspond to the measured RF SNRs, in dB, for the commercial antenna and reconfigurable antenna system respectively. So "mean$(y-x)$" is positive when the reconfigurable antenna is better. "std$(y-x)$" is the standard deviation of $y-x$. r is the correlation coefficient between y and x.

Orientation	No. Transmissions	mean$(y-x)$	std$(y-x)$	r
1	10	+0.2 dB	1.1 dB	+0.95
2	18	+0.1 dB	3.0 dB	−0.26
Combined	28	+0.1 dB	2.5 dB	+0.50

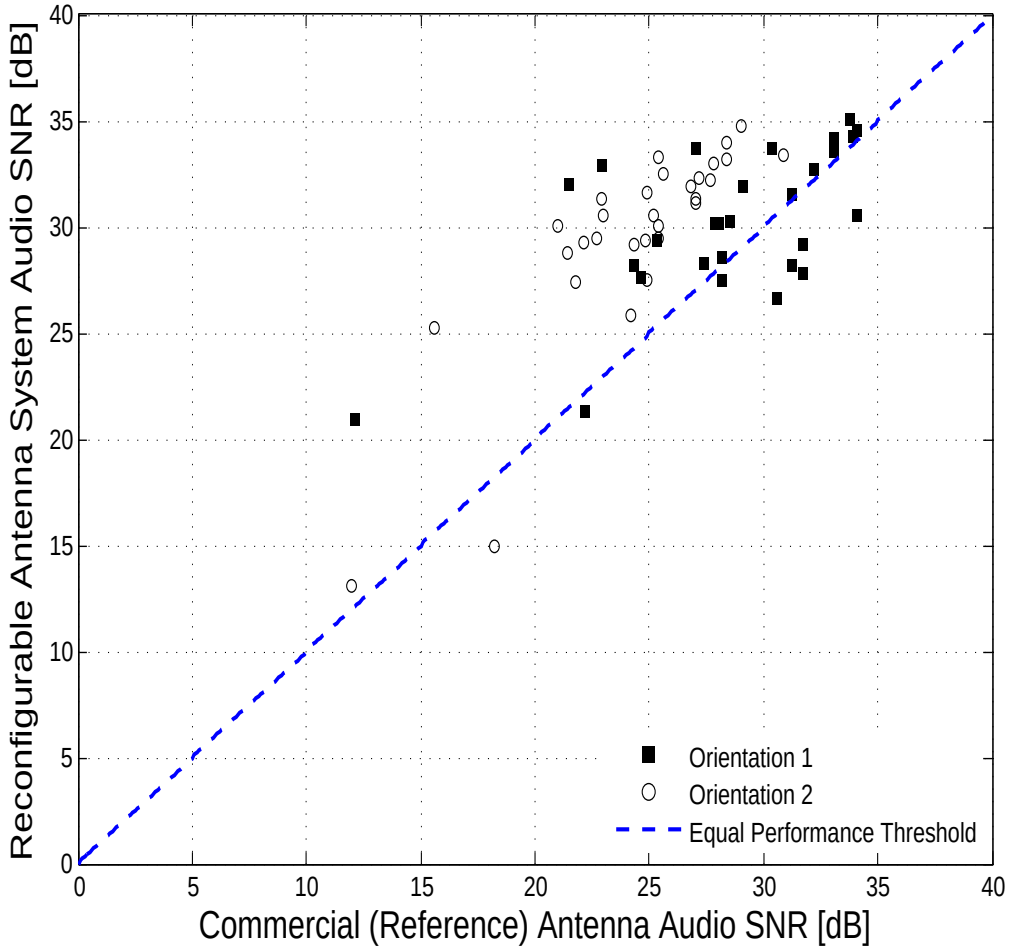

Figure 5.5: 453.625 MHz: Estimated audio SNR for each transmission simultaneously received by both the reconfigurable antenna system and the commercial antenna.

Table 5.4: Statistical analysis of the data in Figure 5.5. x and y correspond to the measured audio SNRs, in dB, for the commercial antenna and reconfigurable antenna system respectively. So "mean$(y-x)$" is positive when the reconfigurable antenna is better. "std$(y-x)$" is the standard deviation of $y-x$. r is the correlation coefficient between y and x.

Orientation	No. Transmissions	mean$(y-x)$	std$(y-x)$	r
1	28	+1.7 dB	3.8 dB	+0.64
2	30	+5.2 dB	2.6 dB	+0.84
Combined	58	+3.5 dB	3.7 dB	+0.69

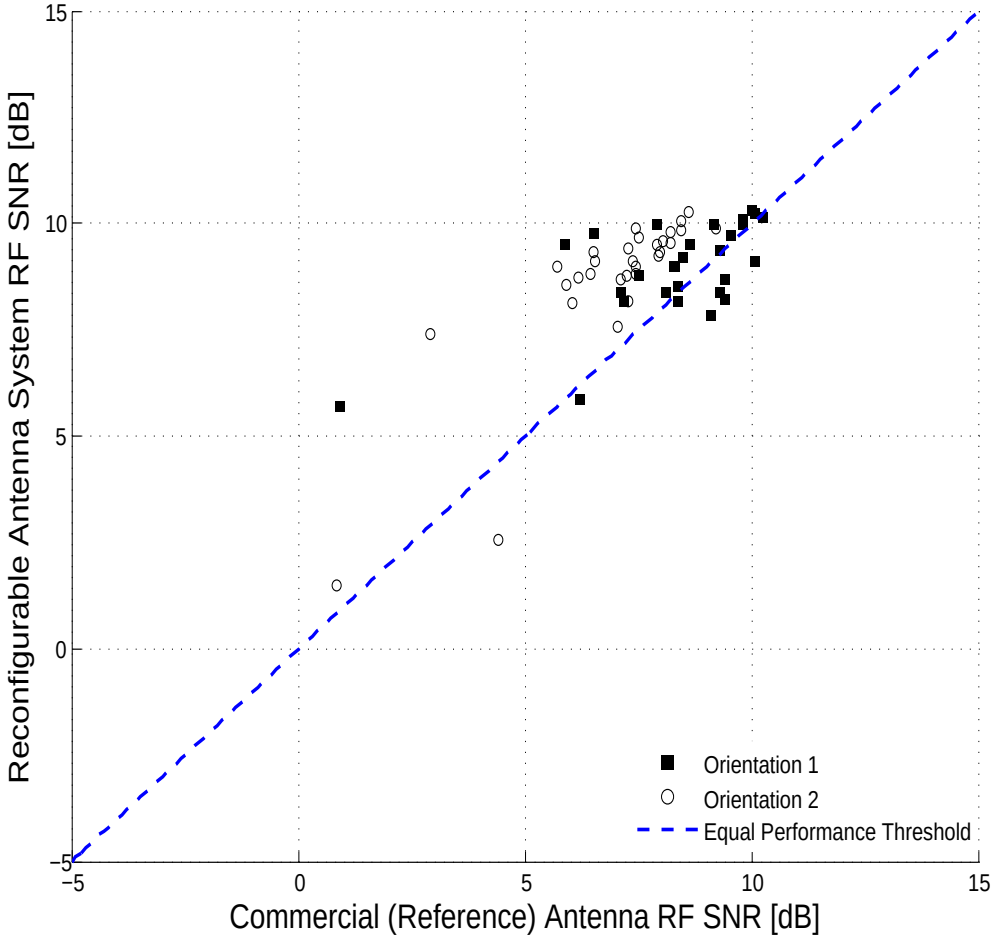

Figure 5.6: 453.625 MHz: Estimated RF SNR for each transmission simultaneously received by both the reconfigurable antenna system and the commercial antenna.

Table 5.5: Statistical analysis of the data in Figure 5.6. x and y correspond to the measured RF SNRs, in dB, for the commercial antenna and reconfigurable antenna system respectively. So "mean$(y-x)$" is positive when the reconfigurable antenna is better. "std$(y-x)$" is the standard deviation of $y-x$. r is the correlation coefficient between y and x.

Orientation	No. Transmissions	mean$(y-x)$	std$(y-x)$	r
1	28	+0.6 dB	1.4 dB	+0.67
2	30	+1.7 dB	1.1 dB	+0.84
Combined	58	+1.2 dB	1.4 dB	+0.72

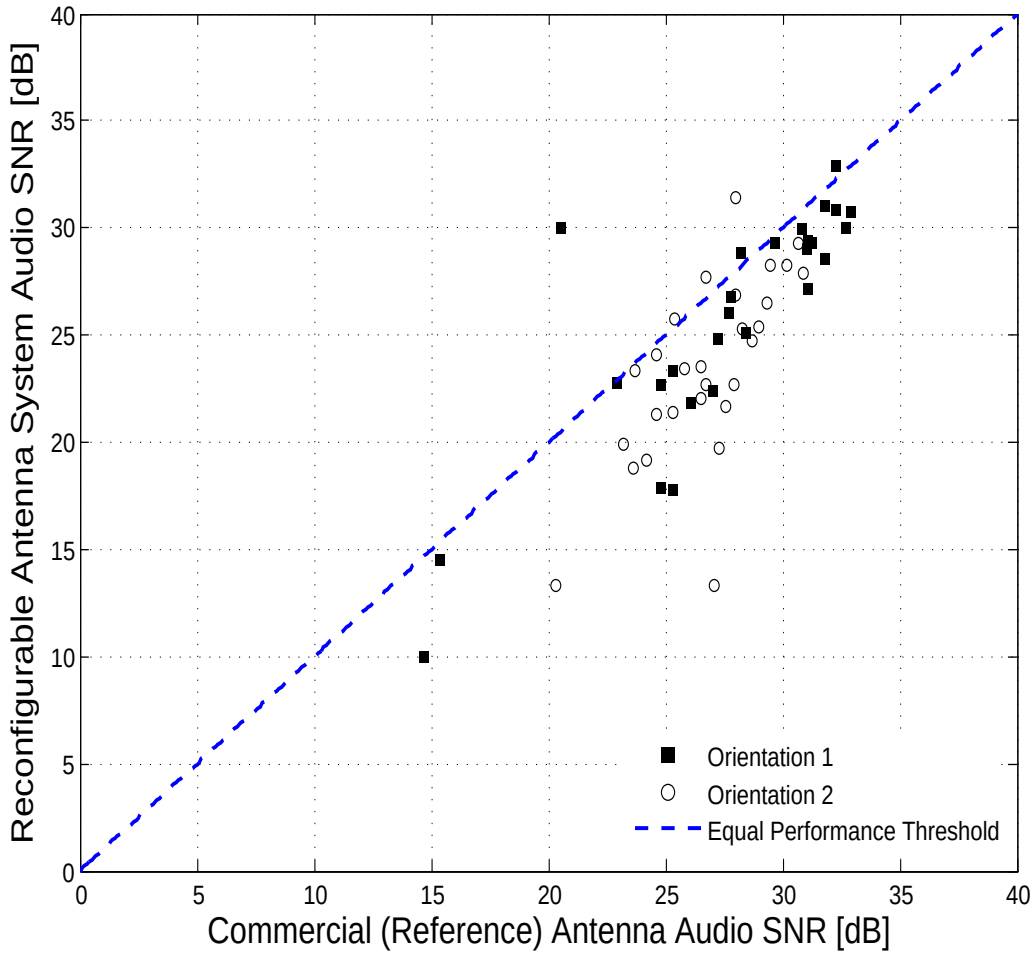

Figure 5.7: 851.150 MHz: Estimated audio SNR for each transmission simultaneously received by both the reconfigurable antenna system and the commercial antenna.

Table 5.6: Statistical analysis of the data in Figure 5.7. x and y correspond to the measured RF SNRs, in dB, for the commercial antenna and reconfigurable antenna system respectively. So "mean$(y-x)$" is positive when the reconfigurable antenna is better. "std$(y-x)$" is the standard deviation of $y-x$. r is the correlation coefficient between y and x.

Orientation	No. Transmissions	mean$(y-x)$	std$(y-x)$	r
1	27	-1.9 dB	3.0 dB	$+0.84$
2	28	-3.3 dB	3.2 dB	$+0.69$
Combined	55	-2.6 dB	3.1 dB	$+0.78$

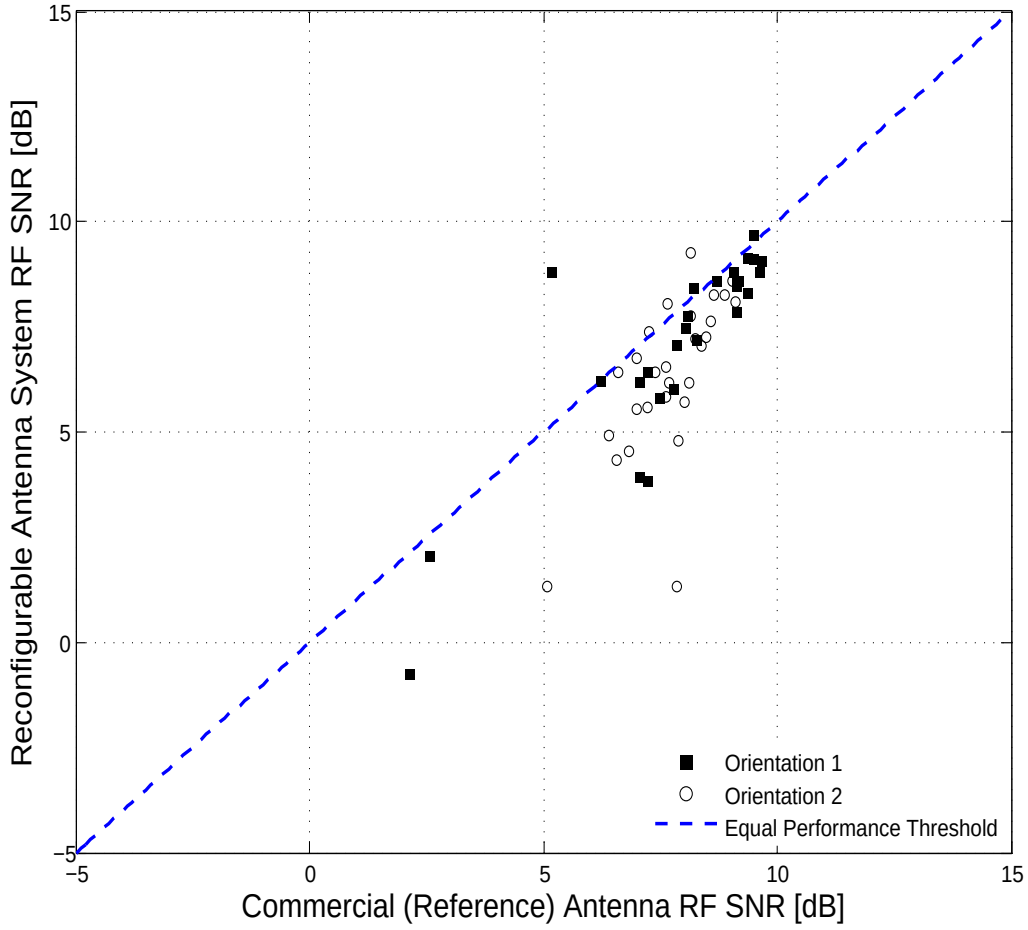

Figure 5.8: 851.150 MHz: Estimated RF SNR for each transmission simultaneously received by both the reconfigurable antenna system and the commercial antenna.

Table 5.7: Statistical analysis of the data in Figure 5.8. x and y correspond to the measured RF SNRs, in dB, for the commercial antenna and reconfigurable antenna system respectively. So "mean$(y-x)$" is positive when the reconfigurable antenna is better. "std$(y-x)$" is the standard deviation of $y-x$. r is the correlation coefficient between y and x.

Orientation	No. Transmissions	mean$(y-x)$	std$(y-x)$	r
1	27	−0.8 dB	1.3 dB	+0.85
2	28	−1.4 dB	1.4 dB	+0.68
Combined	55	−1.1 dB	1.4 dB	+0.78

Chapter 6

Conclusions

This thesis discussed techniques for measurement of antenna performance for analog LMR FM systems. The goal of this thesis was to propose and develop a scheme for *in situ* testing of LMR antennas using PL tone analysis that overcomes the limitations associated with traditional antenna measurement techniques. Specifically, we have developed a technique which allows antennas to be rigorously compared using only audio recordings, and from which relative RF performance can also be determined. We accomplished this goal in this thesis and then evaluated the accuracy of our scheme through simulations, reference experiments and field evaluation of test antennas. The findings of our work are summarized in Section 6.1 ("Findings"). Suggested topics for future research are discussed in Section 6.2 ("Future Work").

6.1 Findings

The principal findings of our research can be summarized as follows:

- *Method for in situ antenna testing*: We proposed and developed methodology for *in situ* characterization of antenna performance in analog LMR FM systems as seen in Sections 1.2, 3.1, 3.2, and 2.3.
- *Characterization of FM audio quality*: We proposed an approach for characterizing the audio quality in LMR analog FM systems. An audio SNR metric that is independent

of the voice signal is obtained by analysis of sub-audio PL tone using the PE/S and kurtosis methods described in Sections 3.1 and 3.2. Sections 3.3, 3.4 and 3.5 present a detailed performance analysis of the PE/S and kurtosis methods through simulations and laboratory experiments respectively. For the simplistic case of a sinusoid in white Gaussian noise, we found that on increasing the integration time, both the methods yield accurate results at lower SNR values. Specifically for an integration time of 100 ms, PE/S method works well for SNR ≥ -30 dB. This is illustrated in Figures 3.1–3.4. For a FM communication system in stationary channel conditions, we found that the PE/S and kurtosis methods are in close agreement with each other for predetection SNR > 5 dB and integration time within a few orders of magnitude of 100 ms. Figures 3.5 and 3.13 presents this result.

- *Estimation of Predetection SNR*: We used the theoretical result presented in Section 2.3 to estimate the predetection SNR from the audio SNR. Sections 4.1 and 4.2 demonstrate the validity of the theoretical result through simulations and laboratory experiments respectively. We found that the experimental result is in close agreement with the simulation result, but the theoretical result follows the measured predetection SNR with a 1–10 dB offset. Figures 4.1, 4.2, 4.4 and 4.6 present these results. Therefore to decrease the offset between the estimated and experimental results, the procedure for estimating the predetection SNR is slightly modified and is outlined in Section 4.3. Following this procedure, we found that the estimated predetection SNR is quite accurate (within 0.5 dB of actual result) for predetection SNR between 3–36 dB. For predetection SNR less than 3 dB, there is a 1–3 dB difference between the estimated and actual value of predetection SNR.

- *Demonstration of the antenna testing methodology*: We demonstrated the proposed antenna testing methodology in Chapter 5 by comparing the performance of an experimental reconfigurable LMR multiband antenna system to that of a commercial antenna in the VHF-Hi, UHF, and 800 MHz bands. The frequency range for each of these bands is listed in Table 2.1. We found that, in the VHF-Hi band, the reconfigurable antenna was on an average, +0.3 dB better than the commercial antenna in terms of audio SNR. This translated into a RF SNR difference of 0.1 dB. The results are shown in Figures 5.3, 5.4 and Tables 5.2, 5.3. We also noted that there was a significant amount of scatter in results due to the time-varying nature of multipath fading. Also we found out that one of the two possible antenna positions was significantly

better than the other. For the UHF band, we noted that the reconfigurable antenna system performed significantly better than the commercial antenna. The performance was +3.5 dB better in terms of audio SNR and +1.2 dB in terms of RF SNR. The results are shown in Figures 5.5, 5.6 and Tables 5.4, 5.5. However for the 800 MHz band, we found that the reconfigurable antenna was on an average, 2.6 dB worse than the commercial antenna in terms of audio SNR and 1.1 dB in terms of RF SNR. The results are shown in Figures 5.7, 5.8 and Tables 5.6, 5.7.

6.2 Future Work

Possible areas to extend the research presented in this thesis are identified and described in this section.

- *Proposed antenna testing method for fading channels*: Our proposed method works well only for stationary (AWGN) and slowly-varying (coherence time $\geq$ 100 ms) channels. However LMR systems sometimes also experience channel conditions with coherence times $\ll$ 100 ms. Therefore we need to modify our method to work well in these conditions and then again evaluate the accuracy of the modified method through simulation and experiments. The modified method would be different from the current method for AWGN channel only in that now a different theoretical result would be needed to estimate predetection SNR from the audio SNR. A theoretical result for estimating predetection SNR from audio SNR under Rayleigh fading conditions is provided in Section 2.4.2.

- *Improving the accuracy of the proposed method*: Although the agreement between the theoretical result for predetection SNR and the simulations (PE/S and kurtosis methods) in Figures 3.5, 4.2, and 4.4 seems to be good enough, it could certainly be improved. To improve the accuracy of the estimate, a possibility is to first determine the audio SNR corresponding to the theoretical predetection SNR using Figure 4.6. Then again using Figure 4.6 determine the simulation predetection SNR corresponding to the measured audio SNR. This value would be the new estimate for predetection SNR.

Bibliography

[1] National Institute of Justice, "Why Can't We Talk? Working Together To Bridge the Communications Gap To Save Lives : A Guide for Public Officials," Feb. 2003. [Online]. Available: `http://www.ojp.usdoj.gov/nij/pubs-sum/204348.htm`

[2] S. W. Ellingson and S. M. Hasan, "What's in Radios Future?: All-band, all-mode radio could solve interoperability challenges." *Mission Critical Communications*, vol. 22, no. 3, pp. 50-60, Mar. 2007.

[3] Joint Tactical Radio System. [Online]. Available: `http://jtrs.army.mil`

[4] Project web site, "Antenna Systems for Multiband Mobile & Portable Radio." Virginia Tech. [Online] `http://www.ece.vt.edu/swe/asmr/`.

[5] W. L. Stutzman and G. A. Thiele, *Antenna Theory and Design*, ch. 1, Wiley, New York, 1981.

[6] Telecommunications Industry Association, "TIA Standard: Land Mobile FM or PM – Communications Equipment – Measurement and Performance Standards", TIA-603-C, Dec. 2004.

[7] W. A. Cumming, "Radiation Measurements at Radio Frequencies: A Survey of Current Techniques", *Proceedings of the IRE*, vol. 47, pp. 705-735, May 1959.

[8] *IEEE Standard Test Procedures for Antennas*, IEEE Std. 149-1979, Published by IEEE Inc., 1979, Distributed by Wiley-Interscience.

[9] W. C. Jakes, ed., *Microwave Mobile Communications*, IEEE press, New Jersey, 1993.

[10] E. N. Singer, *Land Mobile Radio Systems*, Prentice Hall, New Jersey, 1989.

[11] P. Dent, G. Bottomley, and T. Croft, "Jakes fading model revisited," *Electronics Letters*, vol. 29, pp. 1162-1163, Jun. 1993.

[12] T. S. Rappaport, *Wireless Communications: Principles & Practice*, Prentice Hall, New Jersey, 1996.

[13] B. R. Davis, "FM Noise with Fading Channels and Diversity", *IEEE Trans. Comm. Tech.*, COM-19, No. 6, Part II, Dec. 1971, pp. 1189-1199.

[14] S. O. Rice, "Statistical Properties of a Sine Wave Plus Random Noise," *Bell System Tech. J.* 27, pp. 109-157, Jan. 1948.

[15] W. C. Y. Lee, *Mobile Communications Engineering*, ch. 7, McGraw-Hill Inc., New Jersey, 1982.

[16] S. O. Rice, "Noise in FM Receivers," in M. Rowenblatt (ed.), *Proceedings of the Symposium on Time Series Analysis*, Wiley, New York, 1963, Chap. 25.

[17] K. Lee, *Coherent Mitigation of Radio Frequency Interference in 10-100 MHz*. PhD thesis, Virginia Tech., 2008.

[18] R. Matzner and F. Englberger, "An snr estimation algorithm using fourth-order moments," in *Proc. IEEE International Symposium on Information Theory*, p. 119, Jul. 1994.

[19] S. Ellingson, R. Tillman, M. Harun & R. Nealy, "Design and Laboratory Evaluation of the Phase II LMR Multiband Antenna System," Project Report No. 24, Virginia Polytechnic Inst. & State U., June 30, 2012. [online] `http://www.ece.vt.edu/swe/asmr/`.

[20] M. Harun, A. Kumar and S. Ellingson, "Performance comparison of the prototype reconfigurable antenna with commercial LMR antennas," Project Report No. 23, Virginia Polytechnic Inst. & State U., April 10, 2012. [online] `http://www.ece.vt.edu/swe/asmr/`.

[21] M. Manteghi, "Measurement and Analysis of Multiband Mobile Antennas for Portable Radio Applications," Project Report No. 2, Virginia Polytechnic Inst. & State U., July 10, 2010. [online] `http://www.ece.vt.edu/swe/asmr/`